LBNL-48148

ERNEST ORLANDO LAWRENCE BERKELEY NATIONAL LABORATORY

Role of Al on the Microstructure and Mechanical Properties of Hot-Pressed ABC-SiC

Qing Yang

Materials Sciences Division

May 2001

M.S. Thesis

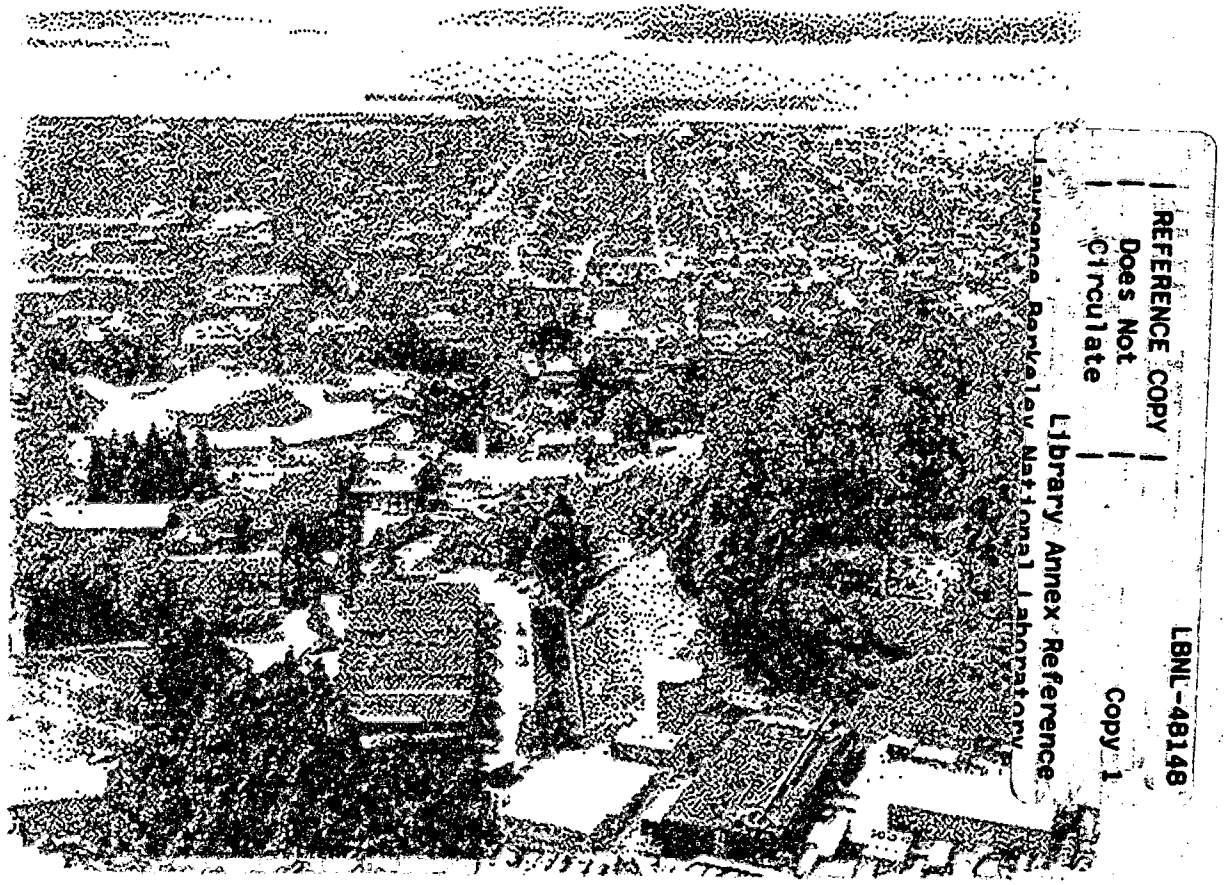

REFERENCE COPY
Does Not
Circulate
Library Annex Reference
Lawrence Berkeley National Laboratory
LBNL-48148
Copy 1

DISCLAIMER

This document was prepared as an account of work sponsored by the United States Government. While this document is believed to contain correct information, neither the United States Government nor any agency thereof, nor the Regents of the University of California, nor any of their employees, makes any warranty, express or implied, or assumes any legal responsibility for the accuracy, completeness, or usefulness of any information, apparatus, product, or process disclosed, or represents that its use would not infringe privately owned rights. Reference herein to any specific commercial product, process, or service by its trade name, trademark, manufacturer, or otherwise, does not necessarily constitute or imply its endorsement, recommendation, or favoring by the United States Government or any agency thereof, or the Regents of the University of California. The views and opinions of authors expressed herein do not necessarily state or reflect those of the United States Government or any agency thereof or the Regents of the University of California.

LBNL-48148

Role of Al on the Microstructure and Mechanical Properties of Hot-Pressed ABC-SiC

Qing Yang
Ph.D. Thesis

Department of Materials Science and Engineering
University of California, Berkeley
and
Materials Science Division
Ernest Orlando Lawrence Berkeley National Laboratory
University of California
Berkeley, CA 94720

May 2001

This work was supported by the Director, Office of Science, Office of Basic Energy Sciences, Materials Sciences Division, of the U.S. Department of Energy under Contract No. DE-AC03-76SF00098.

Role of Al on the Microstructure and Mechanical Properties of Hot-Pressed ABC-SiC

by

Qing Yang

B.E. (Tsinghua University, Beijing, China) 1998

A dissertation submitted in partial satisfaction of the

requirements for the degree of

Master of Science

in

Engineering: Materials Science and Engineering

in the

GRADUATE DIVISION

of the

UNIVERSITY OF CALIFORNIA, BERKELEY

Committee in charge:

Professor Lutgard C. De Jonghe, Chair
Professor Robert O. Ritchie
Professor Claudia P. Ostertag

Spring 2001

TABLE OF CONTENTS

CHAPTER 1: Introduction

1.1 Silicon Carbide Properties 1

1.2 SiC Polytypes 2

1.3 Densification of SiC Ceramics 4

1.4 *In situ* toughened SiC 6

1.5 Al as a Sintering Additive 8

1.6 Objectives 10

1.7 References 12

CHAPTER 2: SiC Ceramic with a Concentration Gradient of Al

2.1 Introduction 15

2.2 Experimental Procedure

2.2.1 Material Processing 15

2.2.2 Hot-Pressing Conditions 17

2.2.3 Characterization 18

2.2.4 Indentation 19

2.3 Results and Discussion

2.3.1 Al Concentration Gradient in the SiC layer 20

2.3.2 Microstructure Change along the Al Concentration Gradient 20

2.3.3 Indentation Toughness and Crack Profiles 24

2.4 Conclusions 27

2.5 References 29

CHAPTER 3: ABC-SiC with Different Amount of Aluminum Addition

3.1 Introduction 30

3.2 Experimental Procedure

3.2.1 Material Processing 30

3.2.2 Microstructure Characterization 31

3.2.3 Mechanical Tests 32
3.3 Results and Discussion
3.3.1 Effect of Al Concentration on Microstructure Evolution 33
3.3.2 Effect of Al wt% on β-to-α phase transformation 38
3.3.3 Correlation between Polytype Transformation, Microstructure Evolution and Additive Content 42
3.3.4 Effect of the Al Content on Grain Boundary Films 45
3.3.5 Secondary Phases and Inclusions 48
3.3.6 Effect of Starting Powders 52
3.3.7 Effect of Microstructure on Mechanical Properties 53
3.4 Conclusions 62
3.5 References 63

CHAPTER 4: Conclusions 65

Acknowledgements

I am extremely grateful to Professor De Jonghe for providing the opportunity to work in his group. I owe him many thanks for supporting this project and providing numerous valuable discussions. Also I would like to thank Dr. Xiao Feng Zhang for guidance, discussion, and all the TEM characterization to facilitate this work.

A special thank and respect to Dr. Da Chen, whose brilliant ideas have helped me a lot in this project. Especially, Da's dedication in his work and his courage in fighting cancer has been inspiring me all the time.

The friendships and advice from the various members of the De Jonghe research group, both past and present, are much appreciated. I am especially grateful for the friendships and help from Dr. Mark Sixta, Caroline Lee, Heeman Choe, and Mr. James Wu.

Finally, I would like to thank my parents, my sister, and my good friends Vivian and Terry McLraith, who have been supporting me with love.

Abstract

Role of Al on the Microstructure and Mechanical Properties of Hot-Pressed ABC-SiC

By

Qing Yang

Master of Science in Materials Science and Engineering

University of California, Berkeley

Professor Lutgard C. De Jonghe, Chair

A systematic study was carried out to investigate the effect of aluminum additive amount on the microstructure development and room temperature mechanical properties of hot-pressed silicon carbide. Two complementary approaches, i.e. varying the aluminum content continuously or by steps, were employed.

An aluminum metal powder compact was placed in a B and C doped SiC green compact, and a continuous aluminum concentration gradient was successfully generated in the SiC after hot-pressing. As the concentration of aluminum decreases, the silicon carbide grains change from (a) elongated with bimodal grain size distribution to (b) uniformly elongated and then to (c) uniformly equiaxed. Both the bimodal region and the elongated region have higher toughness and exhibit extensive crack deflection and crack wake bridging. Regions with more equiaxed grains have a lower fracture toughness.

ABC-SiC with 3wt% to 7wt% aluminum addition were hot-pressed and the effect of the aluminum content on the microstructure and room temperature mechanical

properties was investigated. When the aluminum content varies from 3wt% to 7wt%, the elongated plate-like grains change as follows: the aspect ratio increases about 6 times, the volume fraction of the plate-like grains decreases, the length increases first and then decreases with a maximum at 5wt% aluminum. The microstructural development is related to the change of the grain boundary films from amorphous to crystalline as the aluminum content increases. Room temperature indentation toughness increases with the grain aspect ratio but decreases as the volume fraction of plate-like grains decreases. Fracture strength decreases with increasing grain size. ABC-SiC with 4wt% aluminum addition shows the highest fracture toughness (6.3MPa$\sqrt{m}$) as well as high fracture strength (561MPa).

CHAPTER 1: Introduction

1.1 Silicon Carbide Properties

SiC is a covalently bonded material. The strong covalent bonds between Si and C atoms result in a high decomposition temperature, high elastic modulus, high hardness, and a low thermal expansion coefficient. In addition, SiC has good resistance to oxidation, creep and wear, and has a low density and high thermal conductivity. Furthermore, the raw materials to make silicon carbide are abundant and relatively inexpensive. All these properties make SiC one of the most commonly used structural ceramics.

Historically, silicon carbide is mainly used as an abrasive in bonded wheels and shapes because of its high hardness and refractoriness. Its high thermal conductivity, high decomposition temperature, chemical inertness and low wettability by molten metals also make silicon carbide a useful refractory material. Silicon carbide is used as heating elements, and in ultra-pure doped form is an important high temperature semiconductor. Other applications of silicon carbide include pipe and pump components for corrosive liquids such as HF or NaOH, rocket nozzles, aircraft journal bearings, thrust bearings, etc. Yet other applications that take advantage of the heat-resistant and creep-resistant properties of silicon carbide are aerospace high-temperature rocket nozzle throats, heat-exchangers, furnace controllers, microwave and semiconductor processing fixtures[1], etc. The more exciting and promising expectations are in diesel engines[2,3] and turbine engines[4]. Table 1.1 lists some physical properties of a hot-pressed SiC, and a commercially available pressureless sintered SiC, Hexoloy SA.

Property	Sintered SiC Hexoloy SA	Hot-Pressed SiC
Density (g/cc)	3.10	3.21
Hardness (km/mm^2)	3100	3100
Flexural Strength (MPa)	460	930
Young's Modulus (GPa)	410	440
Poisson's ratio	0.14	~ 0.17
Coefficient of thermal expansion (x 10^{-6}/°C)	4.02	4.8
Thermal conductivity at room temperature (w/m°K)	126	79
Toughness (MPa√m)	2.5	not available

Table 1.1: Physical Properties of SiC.[5]

1.2 SiC Polytypes

SiC has numerous crystallographic variants (polytypes) and more than 200 polytypes have been identified. It is easier to understand the structure of all the polytypes by examining the cubic SiC first. Cubic SiC has a Zincblende structure. Carbon atoms reside at all the corners and face centers of the cube; Si atoms take up four of the tetrahedral sites. The lattice of cubic SiC is f.c.c., where the Si and C "pair" consists of the basis of each lattice point. The close packed {111} planes are a crystallographic abstract of Si-C double layers. The stacking sequence of the double layers in cubic SiC is ...ABCABC.... This cubic phase is denoted as the 3C-polytype (Ramsdell notation) where the number 3 stands for 3 layers in a unit cell and C represents the cubic lattice.

By convention, 3C- polytype is called the β–phase, while the α– phases represent the hexagonal (H) and rhombohedral (R) structures. The variation of the stacking sequence of the Si-C double layer generates the numerous SiC polytypes. The common

(a)

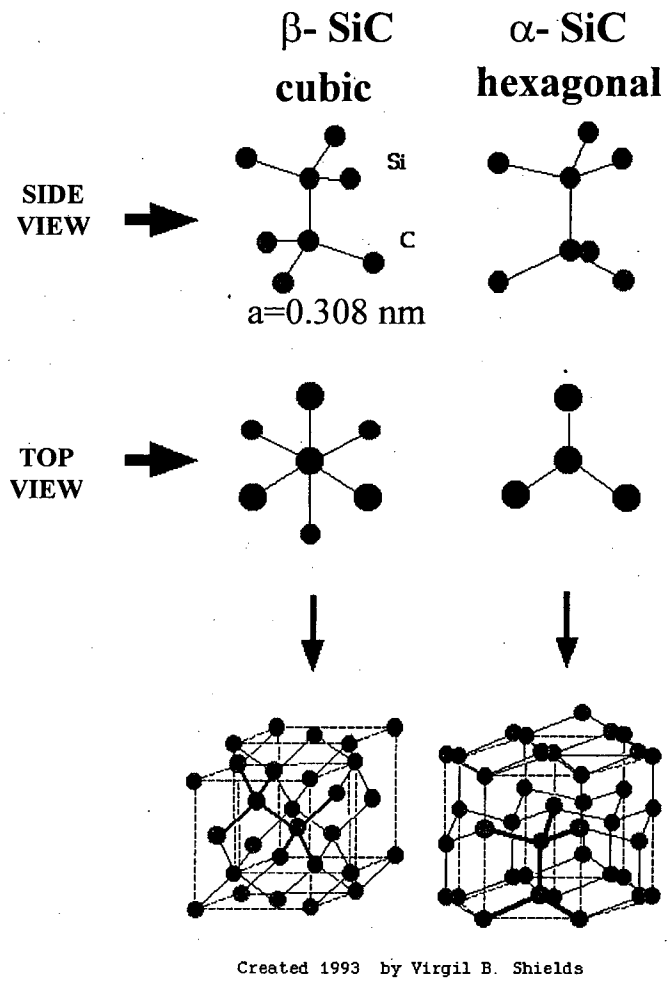

(b)

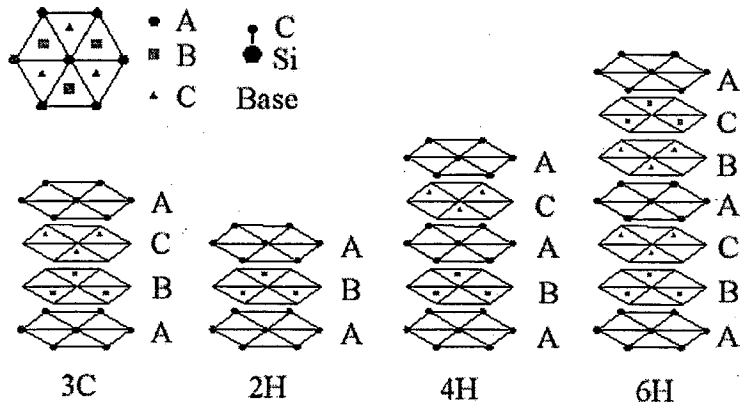

Figure 1-1: (a) [6] Crystal structures and (b) [7] stacking sequence for various SiC polytypes.

α–phases are 4H with the stacking sequence of ...ABAC..., 6H with ...ABCACB... sequence, and 15R with ...ABCBACABACBCACB.... Figure 1-1 shows the crystal structure of SiC and the stacking sequence for some common polytypes .[6,7]

The beta phase is generally considered to be the low temperature phase and α-SiC the high temperature phase. β–phase transforms to one of the various α-polytypes at elevated temperature. Upon subsequent cooling, the microstructure does not revert back to the cubic phase. This is believed to be a kinetically limited process as the α-phases at room temperature are thermodynamically unfavorable. The transformation temperature can be varied by the dopants such as Al, B, etc. The final crystallographic forms of the α-phases are also very sensitive to the type and amount of the additives. It has been found that the presence of boron favors the 6H polytype[8,9,10,11] , whereas 4H usually forms when the environment is rich in Al[9,10,12,13]. The polytype transformations have great importance in the microstructure evolution in SiC ceramics. The effect of additives on the polytype transformation and hence the microstructure will be addressed in more detail throughout this work.

The layers of close-packed planes are the same for the various alpha phases, just the stacking sequence and hence long range order is different. Therefore, the energy difference between the various stacking sequences is very small. This is manifested by a high degree of stacking faults and microtwins that the microstructure of silicon carbides often exhibits. Typically, these planar faults form on one set of the close-packed {111} planes in the β-phase and are parallel to the basal plane in the α-phase.

1.3 Densification of SiC Ceramics

The densification process eliminates free surfaces by forming grain boundaries. Therefore, the thermodynamic driving force for sintering involves the difference between the grain boundary energy and the surface energy. Kinetically, matter has to be transported from the contact area (grain boundary) of the neighboring particles to the neck to eliminate the pores. In polycrystalline materials this process is accomplished through either grain boundary diffusion or lattice diffusion from the grain boundaries to the pores. On the other hand, matter can also be transported from the surfaces of the pores to the neck through lattice/surface diffusion, and through evaporation-condensation. These three routes are non-densification processes, which cause grain coarsening and pore growth.

Although the strong covalent nature of the Si-C bond is the origin of the high elastic modulus, hardness, strength, and chemical stability of SiC, this covalent bond also makes the densification of SiC very difficult. In SiC the difference between surface energy and grain boundary energy is small so the thermal dynamic driving force is limited. The diffusion rate of SiC is also low due to the strong covalent bonds. Given no sintering additives, dense SiC ceramic can be obtained only by hot-pressing at extremely high temperatures (such as 2600°C)[14]. As a consequence, sintering additives are introduced into the SiC system to increase the sintering driving force and sintering rate.

Prochazka *et al.* were the first ones who demonstrated that submicron SiC powder can be pressureless sintered to high density at around 2040°C with less than 1 wt% boron and carbon[15,16]. According to Porchazka *et al.*, boron is found to segregate at the grain boundaries and therefore is believed to lower the grain boundary energy; carbon increases the surface energy by reacting with the native oxide on the SiC particles. Tanaka pointed

out that a certain amount of carbon is required regardless of the oxygen content in the starting SiC powders, suggesting that carbon might also participate in lowering the grain boundary energy.[17]

Another route to achieve high density at relative low temperatures is to introduce a liquid phase during sintering and hence increase the mass transportation rate. For example, Lange[18] (1975) hot-pressed Al_2O_3 doped SiC to high density at 1950°C. Al_2O_3 reacts with the native silica on the surface of SiC powder particles and forms a eutectic liquid at temperatures several hundred degrees lower than the sintering temperature. Mass transportation is greatly enhanced by the liquid phase through a solution-reprecipitation process.[19] The typical densification temperature in liquid phase sintering is in the range of 1800°C to 1900°C, which is significantly lower than that in solid state sintering. Another common liquid-phase sintering additive is Al_2O_3 + Y_2O_3[20,21,22], where Al_2O_3 and Y_2O_3 form yttrium aluminum garnet (YAG). In liquid phase sintering, the densification rate depends on the amount of the liquid, wettability between the liquid and SiC, the size and shape of SiC particles, and the solubility of SiC in the melt.

1.4 *In situ* toughened SiC

Although SiC has many desirable properties, its fracture toughness is low, usually in the range of 2-4 MPa√m. The inherent brittleness of SiC greatly limits the broad application of SiC as structural components where reliability of the part is of great importance. Fortunately, the low fracture toughness of SiC ceramics can be improved by a processing technique called *in situ* toughening.

Suzuki and Sasaki (1987) [23] sintered β-SiC with 5 wt% Al_2O_3 in a high Ar pressure (190 MPa) and got fully densified material with a toughness about 5MPa√m, almost twice of that of traditional sintered SiC with boron and carbon addition. The microstructure of this SiC is a mixture of elongated grains and small grains.[24] As in most liquid phase sintered SiC, grain boundary films were detected along the long edge of the plate-like grains, either glassy or epitaxial crystallized. The grain boundaries are rich in aluminum and on the order of 0.5-2 nm thick.

Padture *et al.* (1994)[25,26] successfully pressureless sintered β-SiC with Y_2O_3, Al_2O_3 and α-SiC seeds and obtained a microstructure of uniformly distributed elongate-shaped α-SiC grains and YAG as intergranular secondary phase. He named the material *in situ* toughened SiC to differentiate the process route from toughening by adding platelets or whiskers. The fracture is intergranular due to the weak glassy phase YAG around SiC grains. The α-seeds facilitate the formation of coarse and elongated grains. The material shows a tortuous crack path and extensive crack-wake bridging. The drawback is the large amount of glassy secondary phase (~20 vol%), which will cause the mechanical properties to be substantially degraded at elevated temperatures.

More recently researchers at Lawrence Berkeley National Laboratory developed ABC-SiC by doping β-SiC powder with a small amount of Al, B, and C and hot-pressing at 1900°C in Ar[27]. The ABC-SiC has high toughness (~9 MPa√m), high fracture strength, excellent oxidation[28], creep[29] and fatigue resistance[30,31] at both room and elevated temperatures. The microstructure consists of elongated plate-like grains that are interlocked together. The as hot-pressed material has ~ 1nm thick amorphous grain boundary films, which crystallize upon post sintering heat treatment[32]. The relatively

weak grain boundary films cause the ABC-SiC to fracture intergranularly and the elongated grains enhance crack deflection, grain bridging, and pull-out[33].

In summary, the common features of *in situ* toughen SiC are elongated grains with high aspect ratio and a weak secondary phases at the grain boundaries. The size and aspect ratio of the elongated grains have a great effect on the mechanical properties.

1.5 Al as a Sintering Additive

As previously mentioned, sintering additives play important roles in processing of SiC ceramics. The ideal sintering additives should:

1) facilitate densification so that high density can be obtained at practically achievable processing conditions,

2) promote the development of elongated grains and weak grain boundary films to enhance the toughness,

3) be effective at a small dose so that the secondary phases will not jeopardize the strength, oxidation and creep resistance at both room and elevated temperatures.

Numerous researches have shown that Al is a very effective additive that can substantially reduce the densification temperature and promote the β-to-α transformation. Alleigro *et al.*[34] hot-pressed α- or β-SiC powder with 3wt% metal elements at 2149°C and found that samples with Al or iron metals achieved the highest density. Bocker *et al.*[9] investigated the pressureless sintering of α-SiC containing various Al compounds and concluded that atomized Al metal is the most effective additive.

The combination of Al, B, and C is also found to be extremely effective, providing enhanced densification at lower processing temperatures. Lin *et al.*[35] reported

in a brief communication that β-SiC was hot-pressed to 96% of theoretical density with a fine-grained microstructure at 1650°C using 6wt%Al metal, 1 wt%B and 1 wt% C-black. Williams and coworkers[12,36] studied in detail the microstructure development in pressureless-sintered β-SiC with Al, B, and C additions. 4H is confirmed to be the favored high temperature form when aluminum is used. 6H and 15R were also detected, but was considered as the intermediate phases of the 3C to 4H transformation. The amount of Al in the study by Williams *et al*[12,36] is about 1.5wt%, higher than the solubility limit of Al in SiC lattice reported by Tajima and Kingery[13]. The excess Al collects in pores and segregates at grain boundaries as an Al-rich second phase, which was identified as mostly $Al_8B_4C_7$.

Some drawbacks of sintering additives require attention. First, although additives such as Al or B lower the sintering temperature to 1700°C, they also cause massive grain growth, which reduces surface areas and intergranular contact, and further densification is retarded[12]. The exaggerated grain growth found in SiC sintered with B+C[11,16] or Al+B+C[37] additives is caused by the extreme anisotropy of the interfacial energy between α- and β-SiC[11,15]. As a result, great care must be taken to avoid overheating or prolonged sintering times. For SiC sintered with oxides, usually a big quantity (>10%) of additives was used[25,38]. Excessive additives are especially detrimental to the high temperature mechanical properties.

More recently Cao *et al.* investigated *in situ* toughened SiC by hot-pressing β-SiC powder with Al, B and C addition[27]. The effectiveness of such combination of additives was confirmed again. Nearly full density was achieved with 3 wt% Al at temperature as low as 1700°C, or with 1wt% Al at 1900°C. The β-to-α transformation in SiC with

3wt%Al-0.6wt%B-2wt%C starts at ~1700°C and is complete at 1950°C. The only α-phase detected is 4H. Quite interestingly, the large amount of Al (comparing to the previous pressureless-sintering cases) does not inhibit the densification in hot-pressing process. No exaggerated grain growth of the α-grains was observed. Instead, the SiC grains are fine and uniformly elongated plate-like grains about 3~8μm long and 7~8 in aspect ratio when hot-pressed at 1900°C for 1 hour.

1.6 Objectives

As mentioned previously, *in situ* toughened SiC has drawn great research interest due to its relatively high toughness compared to traditionally processed SiC. The mechanical properties of *in situ* toughened SiC are in a large part determined by the microstructure. The fracture toughness increases with the aspect ratio of the interlocked plate-like grains; whereas the strength decreases as the grain size increases[27]. To get both high strength and high toughness, the processing conditions have to be controlled judiciously to obtain a microstructure with high aspect ratio and relative small grain size.

It is commonly accepted that aluminum lowers the densification temperature and facilitates the β-to-α transformation and the formation of highly elongated grains. However, little effort has been made to systematically study the correlation between the aluminum content and the microstructure of *in situ* toughened SiC. In this study, the effect of Al metal addition on the microstructure development of the ABC-SiC was investigated. Our purpose is to optimize the microstructure by varying the Al content. Room temperature mechanical tests were carried out to correlate the mechanical properties with the microstructure and to find out the optimal aluminum content. Two

processing approaches were employed to vary the aluminum content either continuously (Chapter 2) or by steps (Chapter 3). Possible mechanisms for the dependence of microstructure evolution with the aluminum content were also proposed.

1.7 References

[1] A. Waugh and B.D. Foster, "Design and performance of silicon carbide cantilever paddles in semiconductor diffusion furnaces," *Cer. Bull.* **64**(4), 550-4, (1985).

[2] P. Rottenkolver, M. Langer, R.S. Storm, and F. Frechette, "Design, Fabrication, and Testing of an Experimental Alpha SiC Turbocharger Rotor," Society of Automotive Engineers, 810 523, (1981).

[3] J. Derby, S.G. MacBeth, and M. Seshadri, "Tribological Behavior of Alpha Silicon Carbide Engine Components," *Conf. Proc.* Paper No. C65/85, pp. 133-37. Institute of Mechanical Engineers, London (1986).

[4] H.E. Helms, P.W. Heitman, L.C. Lindgren, and S.R. Thrasher, *Ceramic Applications inTurbine Engines*. Noyes Park Ridge, NJ. (1986).

[5] M. Srinivasan, "The Silicon Carbide Family of Structural Ceramics," in Structural Ceramics, Edited by J. B. Wachtman, Jr., Treatise on Materials Science and Technology, **29**, 99-159, Academic Press, Inc., (1989).

[6] http://vshields.jpl.nasa.gov/SiC/CubicHex.html

[7] http://www.ifm.liu.se/Matephys/new_page/research/sic/Chapter2.html#2.2

[8] N.W. Jepps and T.F. Page, *Prog. Crystal Growth and Characterization,* **7** 259 (1983).

[9] W, Bocker, R.H. Landfermann, and H. Hausner, "Sintering of Alpha Silicon Carbide Powder with Additions of Aluminum," *Powder Met. Intl.* **11**(2), 83-85 (1979).

[10] R. Hamminger, G. Grathwohl, and F. Thummler, "Microanalytical Investigations of Sintered SiC; Part1, Bulk Materials and Inclusions," *J. Mat. Sci.*, **18** 353-64 (1983).

[11] A.H. Heuer, G.A. Fryburg, L.U. Ogbuji, T.E. Mitchell, and S. Shinozaki,"$\beta \rightarrow \alpha$ Transformation in Polycrystalline SiC:I, Microstrucutral Aspects," *J. Am. Ceram. Soc.*, **61** [9-10] 439-129 (1985).

[12] R.M. Williams, B.N. Juterbock, S.S. Shinozaki, C.R. Peters, and T.J. Whalen, "Effects of Sintering Temperatures on the Physical and Crystallographic Properties of β-SiC," *J. Am. Ceram. Soc.*, **64** [10] 1385-89 (1985).

[13] Y. Tajima and W.D. Kingery, "Solid Solubility of Aluminum and Boron in Silicon Carbide," *Comm. Am. Ceram. Soc.*, **65** [2] C27-29 (1982).

[14] P. L. Farnsworth and R. L. Coble, "Deformation Behavior of Dense Polycrystalline SiC," *J. Am. Ceram. Soc.*, **49** [5] 264-68 (1966).

[15] S. Prochazka and R.M. Scanlan, "Effect of Boron and Carbon on Sintering of SiC," *J. Am. Ceram. Soc.*, **58** [1-2] 72 (1975).

[16] S. Prochazka, "The Role of Boron and Carbon in Sintering of Silicon Carbide," Special Ceramics, Vol. 6, pp. 171-181 (1975).

[17] H. Tanaka, "Sintering of Silicon Carbide," in Silicon Carbide Ceramics--1, Edited by S. Somiya and Y. Inomata, Elsvier Applied Science, NY, NY, pp.213-238, (1991).

[18] F.F. Lange, "Hot-Pressing Behavior of Silicon Carbide Powders with Additions of Aluminum Oxide," *J. Mat. Sci.*, **10** 314-20 (1975).

[19] W.D. Kingery, "Desification during Sintering in the Presence of a Liquid Phase,I: Theory," *J. Appl. Phys.*, **30** [3] 301-06 (1959).

[20] M. Omori and H. Takei, "Pressureless Sintering of SiC," *J. Am. Ceram. Soc.*, **65** [6] C-92 (1982).

[21] R.A. Cutler and T.B. Jackson, "Liquid Phase Sintered Silicon Carbide"; pp.309-18 in *Ceramic Materials and Components for Engines, Proceedings of the Third International Symposium.* Edited by V.J. Tennery. The American Ceramic Society, Westerville, OH, 1989.

[22] M.A. Mulla and V.D. Krstic, "Low-Temperature Pressureless Sintering of β-Silicon Carbide with Aluminum Oxide and Yttrium Oxide Additives," *Ceramic Bulletin*, **70** [3] 439-43 (1991).

[23] K. Suzuki and M. Sasaki, "Pressureless Sintering of Silicon Carbide," presented at Japan-US Seminar on Fundamental Structural Ceramics, Seattle, WA, 1984; *Fundamentals of Structural Ceramics*, edited by S. Somiya and R.C. Bradt, 75-87 (1987).

[24] S.S. Shinozaki, J.Hangas, K.R. Carduner, M.J. Rokosz, K. Suzuki, and N. Shinohara, "Correlation between Microstructure and Mechanical Properties in Silicon Carbide with Alumina Addition," *J. Mater. Res.*, **8**[7] 1635-43 (1993).

[25] N. P. Padture, "*In-Situ*Toughened Silicon Carbide," *J. Am. Ceram. Soc.*, **77**[2] 519-23 (1994).

[26] N. P. Padture and B.R. Lawn, "Toughness Properties of a Silicon Carbide with an *In Situ* Induced Heterogeneous Grain Structure," *J. Am. Ceram. Soc.*, **77**[10] 2518-22 (1994).

[27] J.J. Cao, W.J. MoberlyChan, L.C. De Jonghe, C.J. Gilbert, and R.O. Ritchie, "*In Situ* Toughened Silicon Carbide with Al-B-C Additions," *J. Am. Ceram. Soc.*, **79**[2] 461-69 (1996).

[28] M.E. Sixta, "The Oxidation Behavior of SiC Sintered with Al-B-C and Improved Oxidation Resistance via Heat Treatments," M.S. Thesis. University of California, Berkeley, CA, 1997

[29] M.E. Sixta, "Creep of SiC Sintered with Al, B, and C," Ph.D. Thesis. University of California, Berkeley, CA, 2000.

[30] C.J. Gilbert, J.J. Cao, W.J. MoberlyChan, L.C. De Jonghe, and R.O. Ritchie, "Cyclic Fatigue and Resistance-Curve Behavior of an *In Situ* Toughened Silicon Carbide with Al-B-C Additions," *Acta Materialia*, **44** [8] 3199-214 (1996).

[31] D. Chen, C.J. Gilbert, X.-F. Zhang, and R.O. Ritchie, "High-Temperature Cyclic Fatigue-Crack Growth Behavior in an *In Situ* Toughened Silicon Carbide," *Acta Mater.*, , **48** [3] 659-74 (2000).

[32] X.-F. Zhang, M.E. Sixta, and L.C. De Jonghe, " Grain-Boundary Evolution in Hot-Pressed ABC-SiC," *J. Am. Ceram. Soc.*, **83** [11] 2813-20 (2000).

[33] W.J. Moberlychan, J.J. Cao and L.C. De Jonghe, "The Roles of Amorphous Grain Boundaries and the β-α transformation in Toughening SiC," *Acta Mater.*, **46** [5] 1625-35 (1998).

[34] R.A. Alliegro, L.B. coffin, and J.R. Tinklepaugh, "Pressure-Sintered Silicon Carbide," *J. Am. Ceram. Soc.*, **39** [11] 386-9 (1956).

[35] B.Lin, M. Imai, T. Yano, and T. Iseki, "Hot-pressing of Beta-SiC Powder with Al-B-C Additives," *J. Am. Ceram. Soc.*, **69** [4] C67-C68 (1986).

[36] S.S. Shinozaki, R.M. Williams, B.N. Juterbock, W.T. Donlon, J. Hangas and C.R. Peters, "Microstructure Developments in Pressureless-Sintered β-SiC Materials with Al, B, and C Additions," *J. Am. Ceram. Soc.*, **64** [10] 1389-93 (1985).

[37] D.H. Stutz, S. Prochazka, and J. Lorenz, "Sintering and Microstructure Formation of β-Silicon Carbide," *J. Am. Ceram. Soc.*, **68** [9] 479-82 (1985).

[38] S.K. Lee, and C.H. Kim, "Effects of α-SiC versus β-SiC starting Powders on Microstrucutre and Fracutre Toughness of SiC Sintered with Al_2O_3- Y_2O_3 Additives," *J. Am. Ceram. Soc.*, **77** [6] 1655-58 (1994).

CHAPTER 2: SiC Ceramic with a Concentration Gradient of Al

2.1 Introduction

In this chapter a simple but effective approach is presented to examine the effect of varying aluminum content on the microstructure of hot-pressed SiC. Our goal is to produce a continuous concentration gradient of aluminum in the SiC sample, and to compare the microstructure at different regions of this sample. The concentration gradient is formed during hot-pressing but before the onset of any significant changes such as densification, phase transformation, and grain growth. Another approach that will be discussed in Chapter 3 is the step method, *i.e.* study of a series of samples each of which has a different aluminum content. Comparing to the step method, the continuous method presented in this chapter has several advantages. First, only one sample is needed. Second, since the aluminum content varies continuously, all the possible microstructures will be recorded. Third, all the fluctuations of the experimental conditions can be excluded. The drawback of the continuous method is that it is difficult to separately characterize the properties of different regions. However, it can provide guidance in the selection of aluminum concentration steps for the step method.

2.2 Experimental Procedure

2.2.1 Material Processing

The starting SiC powder was submicron β-SiC powder (H. C. Starck, Grade B20) with a mean particle size of 0.15 μm. The SiC powder was mixed with 0.6 wt% boron (Callery Chemical, Callery, PA), and ~ 4 wt% Apiezon wax (Biddle Instruments, Plymoth Metting, PA). The Apiezon wax was dissolved in toluene, and yielded

approximately 2 wt% C upon conversion by pyrolysis.[1] The slurry of SiC with the additives was ultrasonically agitated for ~ 10 minutes to break up agglomerates, and the mixture was stir-dried in air using a magnetic stir plate. The dried powders were ground using a porcelain mortar and pestle (Coors) and passed through a 200 mesh sieve (maximum particle size is ~ 75 μm).

Different methods were tried to generate a concentration gradient of Al in the SiC. At first Al was sandwiched between two SiC green compacts. However, it was hard to control the proper amount of Al. If the amount of Al is too much, Al is squeezed out and reacts with graphite surrounding the sample. If the amount of Al is too little, it is not enough to produce a nice concentration gradient of Al. An effective approach is to place Al inside SiC powder and then hot-press the sample. First, 1.1 grams of aluminum powder (H-3, atomized, Valimet, Stockton, CA) was cold pressed by uniaxial compression at 35MPa in a steel die set to form a disc 25.4mm in diameter and ~ 1.4mm thick. Then the aluminum disc was buried in 22 grams of boron- and carbon-doped SiC powder. The SiC powder with Al at the center was uniaxially pressed at 35 MPa to form a green compact 38.1mm in diameter and ~ 9mm in height. The cross section of the green compact is illustrated in Figure 2-1.

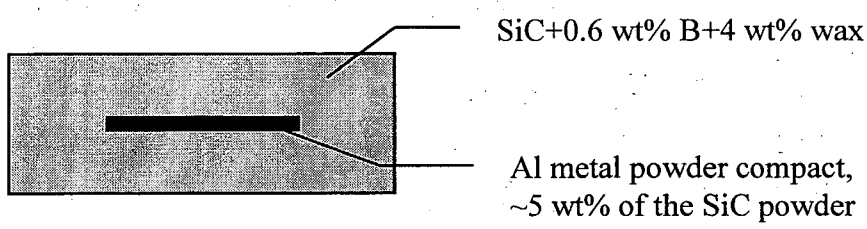

Figure 2-1: Cross section of the green compact before hot-pressing.

2.2.2 Hot-Pressing Conditions

The green compact was hot-pressed in a graphite die lined with graphite foil at 1500°C for 30 minutes and then 1900°C for 1 hour. Figure 2-2 shows the temperature program of the hot-pressing procedure. The purpose of holding at 1500°C is to ensure that enough aluminum has infiltrated into the surrounding SiC green compact. The pressure at the highest temperature was 50MPa. The load was increased at a rate of 1111.3 N/minutes, starting at 1300°C, and was removed at a rate of 666.8 N/minutes, starting at 5 minutes before the end of the 1 hour soak at 1900°C. The atmosphere was flowing Ar gas at 1 psi. The system was heated under manual control to 400°C in vacuum, and pumped overnight to remove the organics and any residual water in the sample. After being backfilled with Ar, the furnace temperature was controlled by a Honeywell controller. The temperature of the furnace was monitored with a W-Rh thermocouple below 1300°C, while a double wavelength optical pyrometer, sighted on the graphite die, was employed for elevated temperatures. The optical pyrometer was

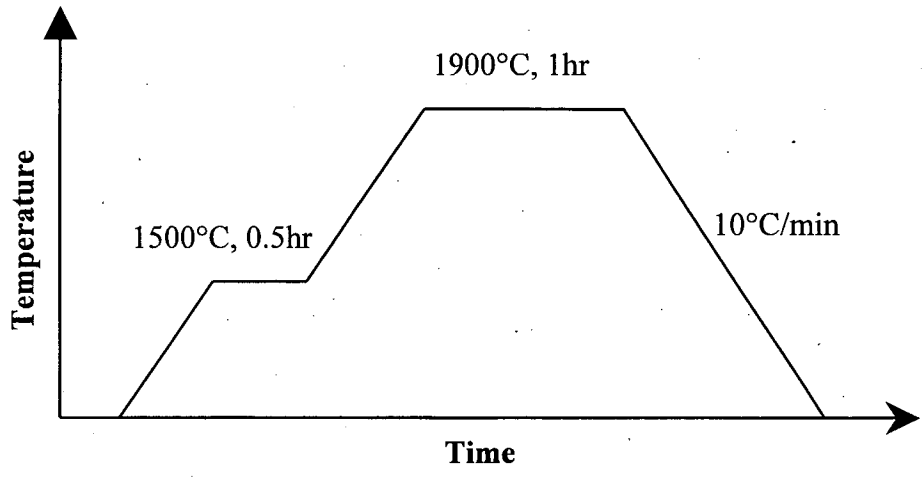

Figure 2-2: Hot-pressing procedure.

calibrated by observing the melting of pure Pt in an alumina crucible and Ar atmosphere.

2.2.3 Characterization

After hot-pressing, the sample was cut along the diameter and was polished using diamond wheels and diamond polishing suspensions of various grades to a 1μm finish. Microstructures were revealed by plasma etching (Plasma-Prep II Model 11005, SPI Supplies, PA) with CF_4+ 4%O_2 as the reactant gas. Plasma etching is routinely used in semiconductor industries. During a plasma etching process, the gas mixture is excited by RF (radio frequency) power and some of the gas molecules are changed into chemically active ions and free radicals. The fluorine free radicals (F^*) react with Si and form gaseous SiF_4[2]. Oxygen enhances the etching rate by forming gaseous phases with carbon and other byproducts. The etch rate of SiC grains and grain boundaries are different due to their different compositions. The SiC grain have a higher etching rate than the silicon deficient grain boundaries because CF_4+O_2 etchant is generally used to etch materials containing silicon, such as silicon dioxide[3] and silicon nitride[4]. The microstructure of SiC was revealed after a 15 minutes etch. Scanning electron microscopy and energy dispersive spectroscopy (EDS) were employed to characterize the grain morphology and the distribution of aluminum.

The plate shape of the SiC grains makes quantifying the grain geometry difficult. In this study, the cross-sectional grain length (l) and width (w) were measured for as many grains as possible (90 to 160) on a SEM micrograph. The mean value of the measured aspect ratio (l/w) was taken to be the apparent aspect ratio. It is worth noting that the length or diameter of a plate-like grain is underestimated because the grain is typically not sectioned through its middle. Conversely, the thickness of a plate-like grain

is exaggerated unless it lies exactly normal to the plane being sectioned. As a result, the aspect ratio determined from two-dimensional measurements tends to be smaller than the actual aspect ratio.

2.2.4 Indentation

Vickers indentation was performed throughout the cross section of the sample to study the effect of microstructure on the crack profile. The cross section was polished to 1μm finish before indentation and was plasma etched to reveal the grains after indentation. Scanning electron microscopy was used to examine the crack profiles.

Indentation toughness was calculated from relations (2-1) and (2-1):

$$K_C = 0.016\left(\frac{E}{H}\right)^{1/2}\left(\frac{P}{C}\right)^{3/2} \qquad (2.1)^{5}$$

$$H = 1.854\left(\frac{P}{d^2}\right) \qquad (2.2)^{6}$$

where P is the peak load, H is the hardness, K_c is the toughness, and E is the elastic modulus. d and c are characteristic dimensions of the indent as shown in Figure 2-3. The elastic modulus E was taken as 430GPa[7] for the calculations. In this study the peak load was 98 N. Values d and c were measured using an optical microscope equipped with a eyepiece scale, whose accuracy is 0.5 μm. All indents were placed at an orientation that two cracks are

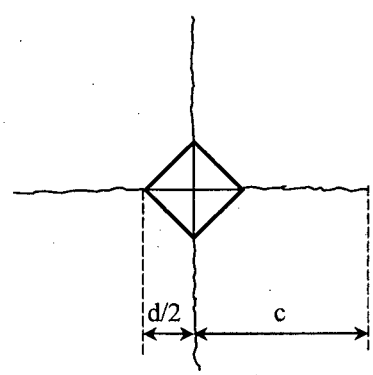

Figure 2-3: Schematic of a Vickers indent.

parallel to the aluminum layer and the other two are perpendicular to the aluminum layer. The distance from the center of the indents to the Al layer was also measured in order to correlate the toughness to the microstructure and Al content.

2.3 Results and Discussion

2.3.1 Al Concentration Gradient in the SiC layer

The hot-pressed sample is ~ 5 mm thick. The thickness of the residual aluminum layer after hot pressing varies from a few microns to ~ 15 μm. EDS was done on the as polished cross section. As shown in Figure 2-4, an aluminum concentration gradient was successfully produced in SiC. The aluminum concentration decreases as the distance to the original aluminum layer increases.

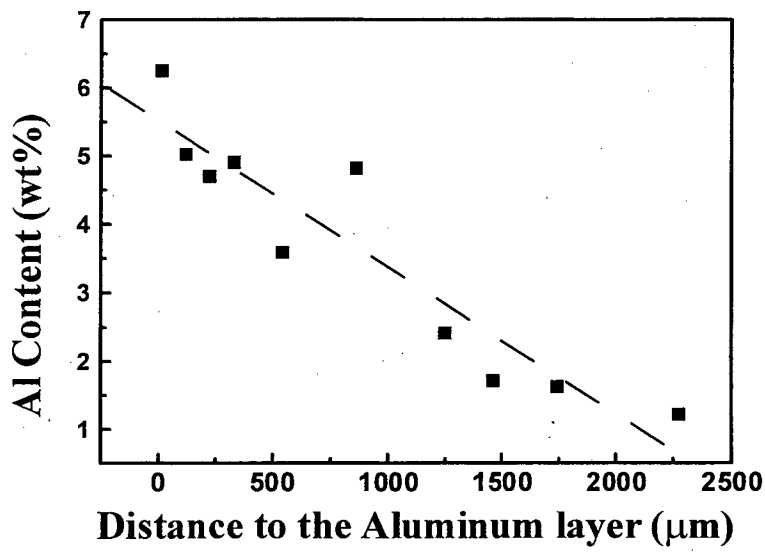

Figure 2-4: Variation of the aluminum concentration in the SiC sample as a function of the distance to the Al layer.

2.3.2 Microstructure Change along the Al Concentration Gradient

Figure 2-5 illustrates the variation of microstructure with the distance to the aluminum layer. According to the different microstructures, the cross-section of the as hot-pressed sample is named by three regions: bimodal region, elongated region and equiaxed region (regions *a, b* and *c* in Figure 2-5 *d*). It is worth noting that although all

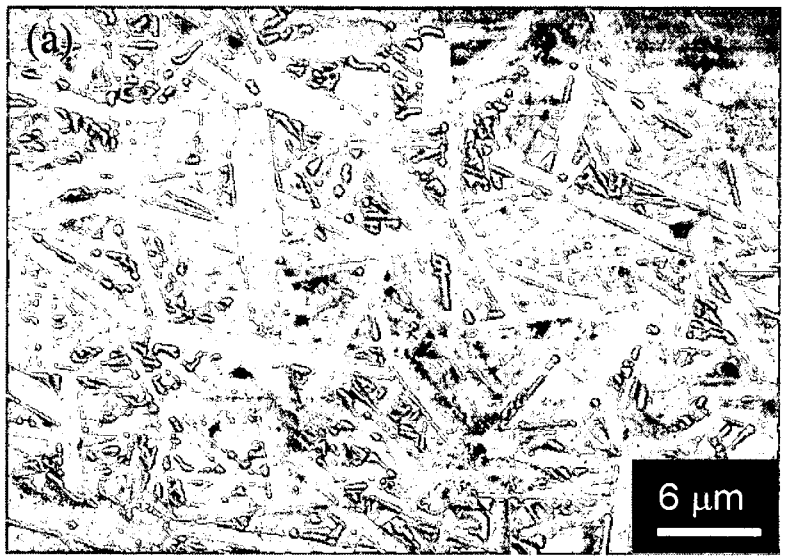

Figure 2-5 Microstructure change in the SiC with the Al concentration gradient. (a) ~ (c) are representative microstructures in regions *a* through *c* as illustrated in the schematic drawing (d).

Figure 2-5 continued.

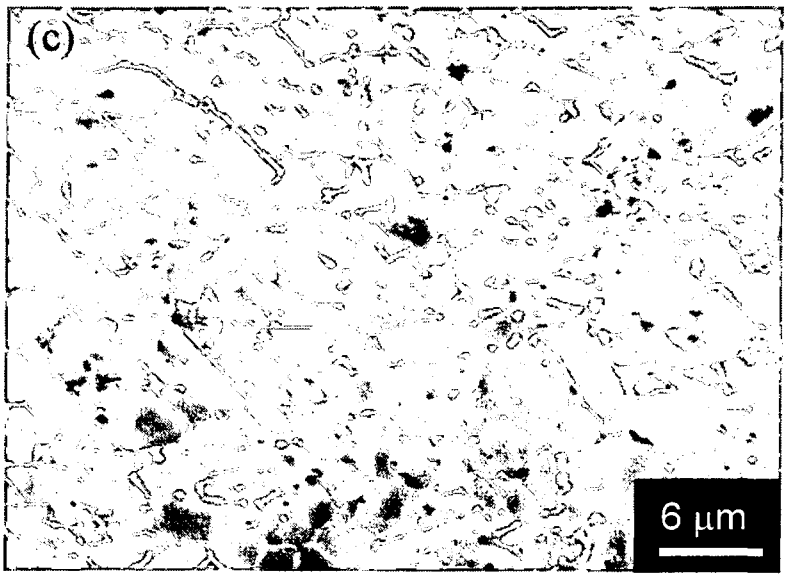

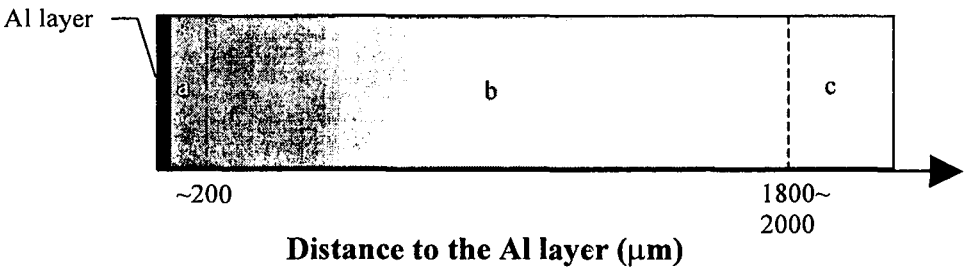

Figure 2-5 (d)

the regions in Figure 2-5 *d* are separated by dashed lines, the actual microstructure varies gradually. In other words, a clear interface between neighboring regions does not exist in the sample. Representative microstructures in the three regions are shown in Figure 2-5 *a* through *c*.

Region *a* is closest to the Al layer and about 200 μm wide. Figure 2-5 *a* shows the microstructure of SiC right next to the original Al layer. The average Al concentration is about 6.3 wt%. Two distinct types of grains exist: big grains and small

grains. The average grain length and width are 8.6 μm and 1.0 μm for the big grains and 4.2 μm and 0.3 μm for the small grains. Although all the grains are elongated, the small grains have higher aspect ratios than the big ones. The average apparent aspect ratio of the big grains is 9.6, about two thirds of that of the small grains (15.4). No exaggerated grain growth was observed.

Region *b* is about 1600 ~ 1800 μm wide. Figure 2-5 *b* shows the typical microstructure in region *b*. The micrograph was taken in the area ~300 μm from the original aluminum layer. The aluminum concentration is about 4.8 wt%. The microstructure resembles the ABC-SiC obtained in an early research by Sixta[8]. Different from region *a*, the grains are almost uniform in size. Compared to the big grains in Figure 2-5 *a*, the length and aspect ratio both decrease by about 40%, with the grain width similar.

Region *c* is the outmost layer, about 500 ~ 700 μm thick. Figure 2-5 *c* was taken in this region and was about 2.3 mm from the original Al layer. The Al concentration is about 1.2 wt% and the grains are mostly equiaxed with an average aspect ratio of 1.7 ± 0.8 and grain length 3.0 ±1.4 μm.

Table 2-1 Grain size and aspect ratio of SiC grains in the three regions.

	length l (μm)	width w (μm)	aspect ratio l/w
Figure 2-5 *a*	4.2 ± 2.0	0.3 ± 0.2	15.4 ± 8.9
	8.6 ± 2.5	1.0 ± 0.4	9.2 ± 3.1
Figure 2-5 *b*	5.5 ± 2.2	1.1 ± 0.5	5.4 ± 2.0
Figure 2-5 *c*	3.0 ± 1.4	1.9 ± 0.9	1.7 ± 0.8

The corresponding grain size and aspect ratios of the three microstructures are summarized in Table 2-1.

No strong EDS single besides background noise could be detected from the black spots in Figure 2-5 *c*, which indicates that these black spots are pores. However, no pores were found in regions *a* and *b*. These regions are rich in aluminum and appear to be fully densified. EDS shows that the dark areas in Figure 2-5 *a* and *b* are aluminum rich secondary phases. The amount of secondary phases in Figure 2-5 *b* is substantially less than in Figure 2-5 *a*, which corresponds to the decreasing aluminum concentration.

2.3.3 Indentation Toughness and Crack Profiles

The microstructure in the SiC sample varies in the direction perpendicular to the aluminum layer. Before calculating the indentation toughness, it is necessary to estimate the area tested by an indent and see whether or not the variation of the microstructure can be ignored. The typical crack length *c* is about 100 μm for *in situ* toughened SiC. So the region being tested by the indent is about 200 μm wide, which is comparable to the width of region *a*. This means that the variation of the microstructure can not be ignored. Cracks from different corners of an indent experience different environments. A crack propagating towards the aluminum layer "sees" increasing aspect ratios and grain sizes. In contrast, a crack propagating away from the aluminum layer develops into area with smaller and smaller aspect ratios and grain sizes. As a consequence, the toughness obtained from an indent in region *a* does not correspond to a certain microstructure; rather, it is some "average" value over the gradually changing microstructures.

Given the size of the indentor, it is not possible to get the true indentation toughness values of the different regions in this gradient SiC. However, we can still qualitatively evaluate the effect of microstructure on the toughness by comparing the values calculated using Equation (2-1). Figure 2-6 shows the variation of the indentation toughness vs. the distance to the Al layer. Most of the data points fall into a band as depicted by the shadowed area. The band may suggest the general trend that the indentation toughness decreases with the decreasing Al content. Within ~1100 μm to the Al layer, most of the indentation toughness values are about 6 to 8.5 MPa√m. Two factors may account for the high toughness: 1) elongated plate-like grains, especially the unique bimodal region; 2) the high residual Al content. The toughness value drops to ~ 4.5 MPa√m in the region (~1400 to 1600 μm) that contains equiaxed grains and low Al content. Several points in Figure 2-6 that located at ~260μm have higher than usual

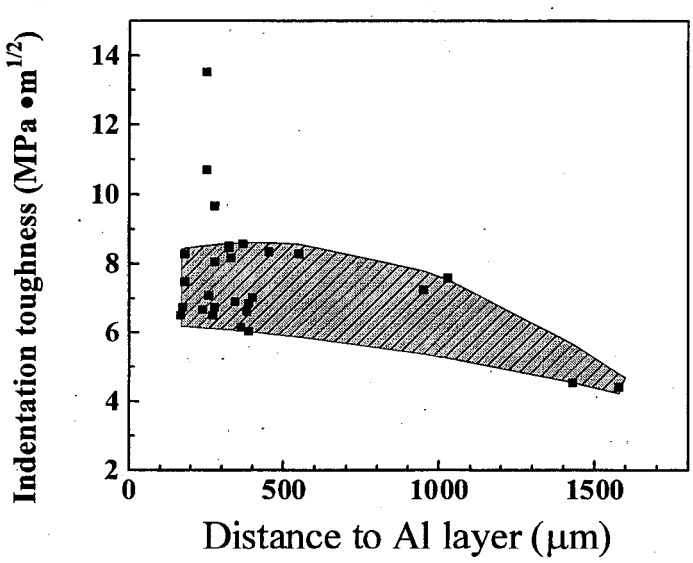

Figure 2-6: Variation of the apparent indentation toughness value as a function of the position to the Al layer.

toughness values and are outside of the band. This may be caused by the residual metallic Al secondary phases. As a semi-elliptical crack from a Vickers indent propagates, it may encounter these residual metallic Al phases, which deform plastically. This may suggest that a ceramic-metal composite with *in situ* toughened SiC matrix may have a combination of high strength and high toughness.

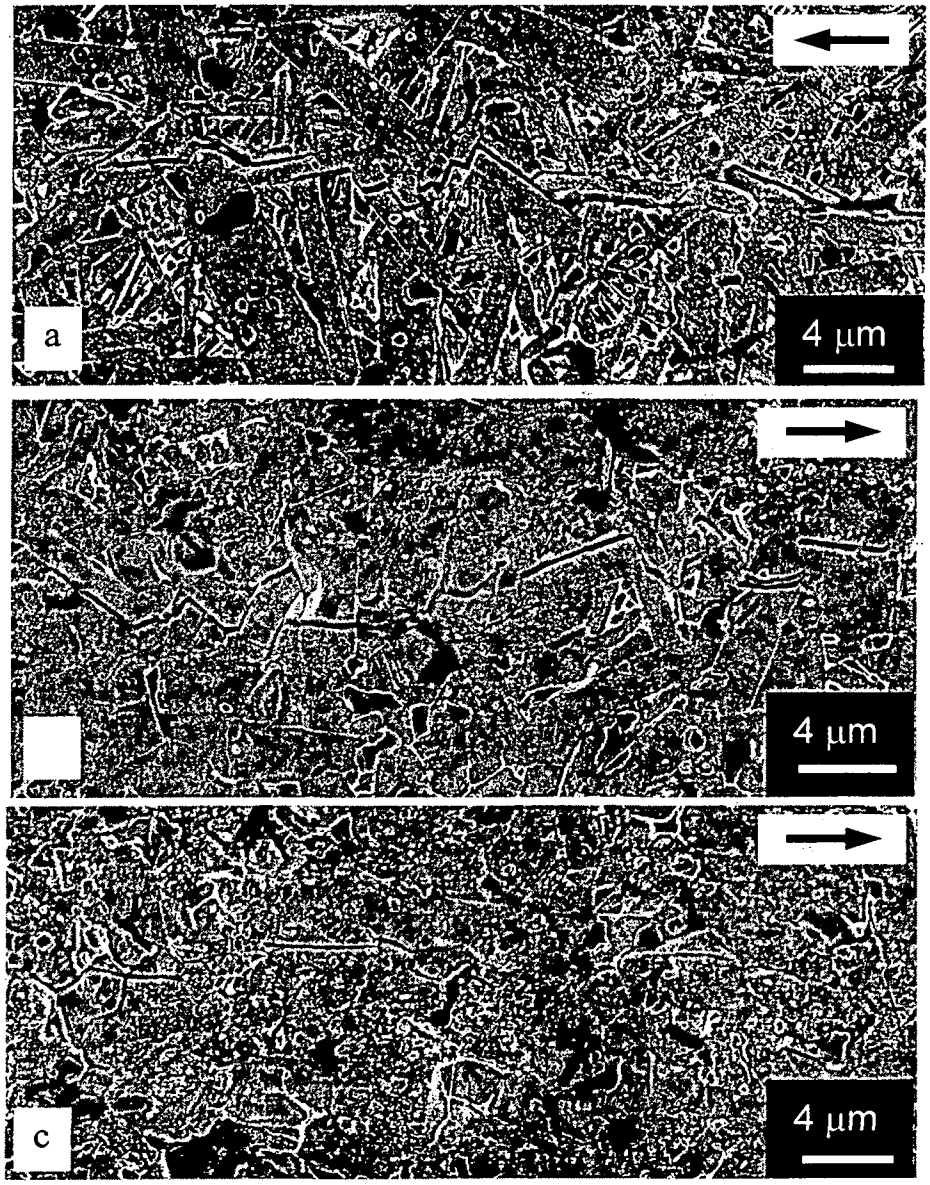

Figure 2-7: SEM micrographs of crack paths in (a) region *a*, (b) region *b*, and (c transition area between region *b* and *c*. Note the difference in the grain size an aspect ratio. The horizontal arrow shows the direction of crack growth.

Crack profiles have been widely used as a simple and convenient approach to observe crack-microstructure interaction in ceramics. For example, cracks in an *in situ* toughened ABC-SiC show extensive crack deflection at the grain boundaries and grain bridging; by contrast, cracks in a low toughness SiC* are straight and transgranular, with no indication of crack-wake bridging[9]. Cracks at different locations of the SiC sample are compared in Figure 2-7. Plasma etching of the polished cross section after indentation reveals the interaction between microstructure and crack profiles. Figure 2-7 *a* and *b* are taken in the regions *a* and *b*, respectively. Extensive crack deflection at the grain boundaries and many grain bridging sites are evident in Figure 2-7 *a* and *b*. In contrast, the crack shown in Figure 2-7 *c* develops mostly transgranularly and is much straighter, which indicates a low fracture toughness.

2.4 Conclusions

A continuous aluminum concentration gradient was successfully generated in SiC ceramic by hot-pressing a sample with an aluminum metal powder compact enclosed in B- and C-doped SiC powder. The microstructure as well as the mechanical properties of SiC change with the distance to the original aluminum layer.

Three regions were named according to the microstructure difference: bimodal region, elongated region, and equiaxed region. Representative microstructures of each region are shown in Figure 2-5 and summarized in Table 2-1.

Both the bimodal region and the elongated region have higher toughness. The crack profiles show extensive crack deflection and crack wake bridging. On the other

* Commercial SiC (Hexoloy SA) from Carborundum, Niagara Falls, NY.

hand, regions with more equiaxed grains have lower fracture toughness. The cracks are transgranular and straight.

Furthermore, this study demonstrates a simple but effective way to investigate the qualitative aspect of additive composition on the microstructure development and the microstructure-crack interaction.

2.5 References

[1] J. Cao, "*In situ* Toughened SiC Ceramics with Al-B-C Additions and Oxide-Coated SiC Platelet/SiC Composites," Ph.D. Thesis, University of California, Berkeley, pp. 22, (1996).

[2] W.R. Runyan and K.E. Bean, Semiconducto Integrated Circuit Processing Technology, pp274-7, Addison-Wesley, 1990.

[3] A.R. Reinberg, *Etching for Pattern Definition*, pp91, Electrochemical Society, Princeton, N.J., 1976.

[4] D.L. Flamm *et al.*, *Electrochem. Soc. Ext. Abst.* 81-2, abst. no. 270, 1981.

[5] G.R. Anstis, P. Chantikul, B.R. Lawn, and D.B. Marshall, "A Critical Evaluation of Indentation Techniques for Measuring Fracture Toughness: I, Direct Crack Measurements," *J. Am. Ceram. Soc.*, **64** [9] 533-38 (1981).

[6] I. Merkel and U. Messerschmidt, "Fracture Toughness of Sintered SiC Ceramics: a Comparison between Different Methods," *Materials Science and Engineering*, **A151**, 131-5 (1992).

[7] *ASM Handbooks*, ASM International, Materials Park, Ohio.

[8] M.E. Sixta, "Creep of SiC Sintered with Al, B, and C," Ph.D. Thesis. University of California, Berkeley, CA, 2000.

[9] J.J. Cao, W.J. MoberlyChan, L.C. De Jonghe, C.J. Gilbert, and R.O. Ritchie, "*In situ* Toughened Silicon Carbide with Al-B-C Additions," *J. Am. Ceram. Soc.*, **79**[2] 461-69 (1996).

CHAPTER 3: ABC-SiC with Different Amount of Aluminum Addition

3.1 Introduction

The method presented in Chapter 2 is a simple way to study the effect of aluminum content on the microstructure of SiC. It also provides guidance on the range of aluminum concentration selected for further study. However, because the microstructure varies continuously, lots of important information such as polytypical composition, strength and toughness are difficult to obtain. In this chapter, a series of SiC samples with homogeneously distributed aluminum addition will be discussed.

As mentioned previously, the mechanical properties of *in situ* toughened SiC are in a large part determined by the microstructure. The fracture toughness increases with the aspect ratio of the interlocked plate-like grains; whereas the strength decreases as the grain size increases[1]. The ideal microstructure will be one that has a high aspect ratio and moderate grain size. The purpose of this study is to find out the optimal aluminum content that facilitates the formation of high aspect ratio grains without causing massive grain growth. Possible mechanisms of the microstructural changes with the aluminum content will also be proposed to provide better understanding for the basics of microstructure control.

3.2 Experimental Procedure

3.2.1 Material Processing

The starting SiC powder was high purity cubic β-SiC (BETARUNDUM, Grade ultra-fine, IBIDEN, Japan) with a mean particle size of 0.27 μm. The SiC powder was mixed with 3 wt% to 7wt% aluminum metal powder (H-3, Valimet, Stockton, CA), ~ 3

μm average particle size, and 0.6 wt% boron, and ~ 4 wt% Apiezon wax, which yielded approximately 2 wt% C by pyrolysis.[1] The slurry was ultrasonically agitated, stir-dried and sieved through a 200 mesh screen. The sieved powder was cold pressed at 35MPa and loaded into a graphite die. A maximum of three disks were sintered at a time, enclosed in graphite foils and separated by graphite spacers. The hot-pressing conditions are exactly the same as in Chapter 2. The hot-pressed disks were 38 mm in diameter and ~ 4 mm thick.

3.2.2 Microstructure Characterization

The surfaces of the hot pressed pellets were ground off by ~ 500 μm using a surface grinder with a diamond wheel. One side of each sample was then polished to a 1μm finish. The densities of the specimens were determined by the Archimedes method. Theoretical densities of the materials were calculated according to the rule of mixture. X-ray diffraction (XRD) was carried out on the polished surfaces of the disks over the range $2\theta = 20°$ to $80°$ at steps of 0.05°, with a time constant of 1 second. The quantity of the SiC polytypes in specimens was calculated using the series of equations presented by Ruska *et al.*, [2] which are listed in Table 3-1. The capital letters **A** to **F** stand for the intensities of the diffraction corresponding to the *d* spacing listed in the last column of Tabel 3-1. The peak intensities were determined by integrating the areas under the peaks, with background being subtracted first; **a** to **d** are the unknown quantities to be solved. They are related to the amount of each polytype: a for 15R, b for 6H, c for 4H, and d for 3C. A numerical method was employed to find the best fit of the equations. Solutions were double-checked by comparing them with the experimental diffraction spectra.

15R		6H		4H		3C	Peak	d(nm)
3.2**a**			+	9.9**c**			= **A**	0.266
11.2**a**	+	19.4**b**					= **B**	0.263
26.0**a**			+	38.9**c**			= **C**	0.257
31.1**a**	+	59.2**b**	+	25.1**c**	+	100.0**d**	= **D**	0.251
		18.1**b**	+	34.1**c**			= **E**	0.235
2.4**a**	+	6.5**b**			+	13.1**d**	= **F**	0.217

Table 3-1: Equations to calculate the SiC polytypes.[2]

Microstructures of the hot-pressed materials were studied by scanning electron microscopy (SEM) on polished and plasma etched surfaces, which were perpendicular to the direction of the load during hot-pressing. Surfaces parallel to the loading direction were also examined and no texture was observed. Microstructure characteristics, including the grain size, aspect ratio, and size distribution, were evaluated using the same method as mentioned in Chapter 2. For the microstructures with bimodal grain size distributions, area densities of different types of grains, defined as number of grains per unit area, were used to describe quantitatively the microstructure. The aluminum distribution was determined by EDS. Conventional and high resolution transmission electron microscopy (TEM and HR-TEM) was performed to study the polytypes, grain boundaries and grain morphology.

3.2.3 Mechanical Tests

Four point bend strength were evaluated on beams of ~ 3 mm by 3 mm by 30 mm sectioned from the polished disks. The tensile edges were beveled using a 6 μm diamond

wheel to reduce the edge flaws. The flexural strength was tested using a four-point bending jig with an inner span of 9.5 mm and an outer span of 25.4 mm. The crosshead speed during the test was 0.05 mm/minute and the modulus of rapture (MOR) was calculated from the following relation:

$$\sigma = \frac{3Pa}{bh^2} \tag{3-1}$$

where σ is the four-point bend strength, P is the load at fracture, a is one-half of the distance between the inner and outer spans, b is the width of the beam, and h is the height of the beam. The bend strength for every aluminum content was averaged over at least six beams.

Fracture toughness was estimated by Vickers indentation method with a peak load of 98 N. At least six indents were measured for each aluminum composition. Details of the indentation experiment have been provided in Chapter 2.

SEM was used to examine the fracture surfaces and the crack profiles on indented and then plasma etched specimens.

3.3 Results and Discussion

3.3.1 Effect of Al Concentration on Microstructure Evolution

Table 3-1 lists the compositions of samples and densities after hot-pressing. Samples were named according to additive content. A, B, and C stand for aluminum, boron, and carbon, respectively. The number designates the Al wt%. Densities greater than 99% theoretical density were reached for all samples. SEM micrographs taken on the plasma-etched surfaces of each sample were shown in Figure 3-1 *a* through *e*. The five silicon carbide materials show four distinctly different microstructures, with 6ABC-

SiC and 7ABC-SiC having similar features. As the aluminum content was increased by only 4wt%, the aspect ratio and size of elongated plate-like grains as well as the volume fraction of the elongated grains all changed drastically. It is worth noting that the aspect ratios of the elongated grains in 4ABC-SiC to 7ABC-SiC are very high, in the range of 20 to 45, but the grain size is relatively small (less than 50μm). Although rapid gain growth did occur for some aluminum contents, no abnormal grain growth[3,4,5,6] was found in our materials.

Sample Designation	SiC (wt%)	Al (wt%)	Density(g/cm^3)
3ABC-SiC	94.4	3	3.18
4ABC-SiC	93.4	4	3.24
5ABC-SiC	92.4	5	3.25
6ABC-SiC	91.4	6	3.13
7ABC-SiC	90.4	7	3.15

All samples also contain 0.6 wt% B and 2 wt% C.

Table 3-2: Compositions and densities of samples

Slightly varying the aluminum content can drastically change the aspect ratio and length of the elongated plate-like grains. As shown in Figure 3-2 a, the average aspect ratios of elongated plated-like grains increase from about 5 to over 30 as the aluminum content changes from only 3 wt% to 7 wt%. Figure 3-2 b shows the variation of the lengths of the plate-like grains with the changing of the aluminum content. The grain length first increases from 4.4 μm to 20 μm as the Al wt% increases from 3 wt% to 5 wt%, then drops to 9.1 μm as the aluminum content changes to 6 wt%, and slightly increases when Al reaches 7 wt%. 5ABC-SiC shows the longest elongated grains and 3ABC-SiC the shortest. Comparing 4ABC-SiC with 3ABC-SiC, both the lengths and the

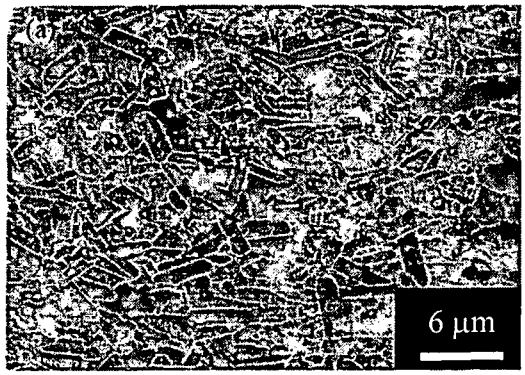

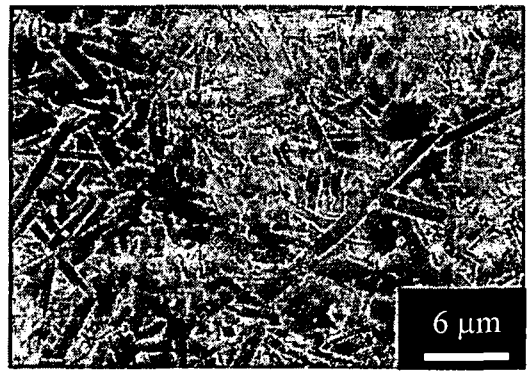

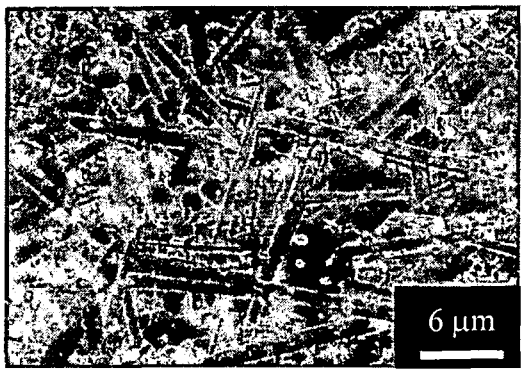

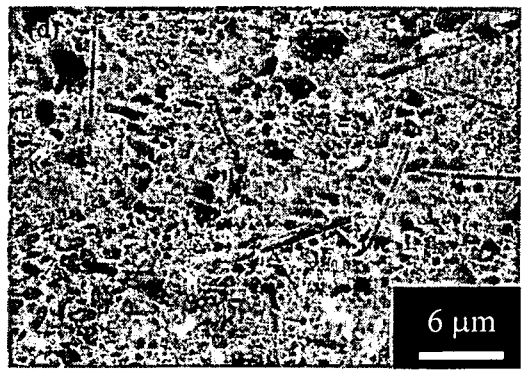

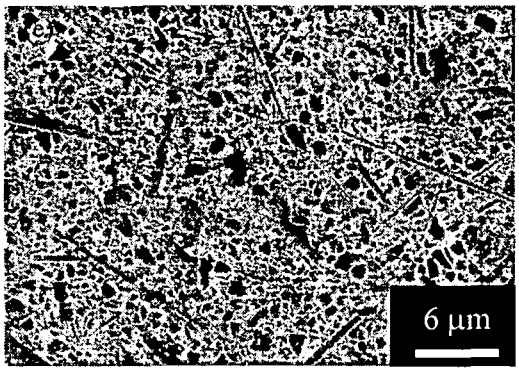

Figure 3-1: SEM micrographes showing the microstructures of (a) 3ABC-IBD, (b) 4ABC-IBD, (c) 5ABC-IBD, (d) 6ABC-IBD, (e) 7ABC-IBD

aspect ratios of plate-like grains of 4ABC-SiC are 4 to 5 times of those in 3ABC-SiC, although the aluminum content is raised by only 1 wt%. The thickness of the plate-like grains is similar, about 1 μm, in samples with 5wt% and lower aluminum content. 6ABC-SiC and 7ABC-SiC possess thinner plates (about 0.3 to 0.4 μm thick). Although

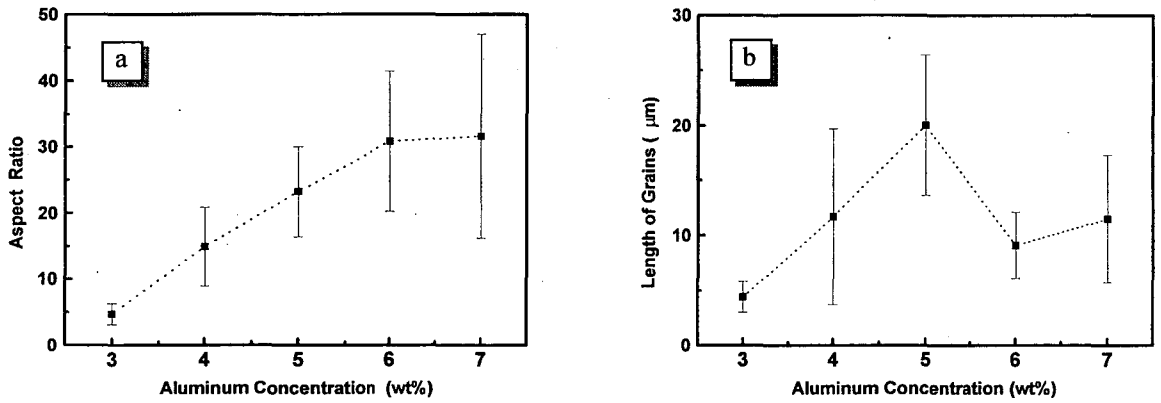

Figure 3-2: Effect of the aluminum concentration on (a) the aspect ratio and (b) the grain size of SiC.

the lengths of the elongated plate-like grains in 6ABC-SiC and 7ABC-SiC are comparable to the grain length of 4ABC-SiC and about half of that of 5ABC-SiC, the smaller plate thickness results in a big increase in the aspect ratios of those elongated grains in 6 and 7 ABC-SiC. The results of grain morphology analysis were summarized in Table 3-3.

Table 3-3: Results of Microstructural Analysis

Material	Elongated Plate-like Grains			Equiaxed Grains d (μm)	Area Density of Elongated Grains (mm^{-2})
	length l (μm)	width w (μm)	aspect ratio l/w		
3ABC-SiC	4.4 ± 1.4	1.0 ± 0.3	4.7 ± 1.6	—	85,000
4ABC-SiC	11.7 ± 8.0	0.8 ± 0.5	14.9 ± 6.0	0.5 ± 0.3	57,000
5ABC-SiC	20.0 ± 6.4	0.8 ± 0.3	23.2 ± 6.8	0.6 + 0.2	45,000
6ABC-SiC	9.1 ± 3.0	0.3 ± 0.2	30.8 ± 10.6	0.5 ± 0.3	25,000
7ABC-SiC	11.5 + 5.8	0.4 + 0.2	31.6 + 15.4	0.6 ± 0.3	23,000

Increasing the Al wt% not only affects the size and shape of elongated plate-like grains of SiC, but also results in the variation of the volume percentage of the elongated

grains. As shown in Figure 3-1 *a*, 3ABC-SiC has slightly elongated grains with a uniform grain size; whereas in 4ABC-SiC a few submicron equiaxed grains can be detected. 5ABC-SiC has more equiaxed grains distributed in the network of elongated grains, and the equiaxed grains become dominant in 6ABC-SiC and 7ABC-SiC. In a word, all the other materials besides 3ABC-SiC show bimodal grain size distributions. The area density of the elongated grains as a function of the aluminum content is also listed in Table 3-3 to reflect this change. The result demonstrates that sufficient aluminum actually inhibits the formation of elongated plate-like grains. High aspect ratio grains can be obtained without encountering severe grain growth.

The fracture toughness of ceramics can be improved by incorporating rod-like or plate-like reinforcements that generate a bridging zone in the crack wake[7], as has been demonstrated in numerous studies on *in situ* toughened silicon nitride and silicon carbide. However, the large reinforcement grains could readily act as flaws and result in degrading the strength. Most *in situ* toughened silicon carbides show a trade-off in improving both fracture strength and fracture toughness[8]. Producing a bimodal grain size distribution can be a promising route to improve the stead-state fracture toughness without sacrificing the high strength of ceramics. Becher et al. [9] judiciously controlled the microstructure of a silicon nitride and achieved a fracture toughness 10 MPa$\sqrt{m}$ and fracture strength in excess of 1 GPa. The silicon nitride has a distinct bimodal distribution of grain diameters and well dispersed elongated grains. In contrast, if a broad grain diameter distribution is generated, both the fracture toughness and fracture strength undergoes a substantial reduction[9,10]. Many *in situ* toughened silicon carbide ceramics also show bimodal grain size distributions[8,11,12]. However, the strength of these silicon

carbide was either not reported or low. This is presumably because of the large amount of additives (10~20wt%). Seeding[8,11] and prolonged post sintering annealing[12] were commonly employed strategies to obtain a bimodal grain size distribution in SiC. In the current study, the bimodal grain size distribution can be generated by simply varying the aluminum content in the starting β powder, with a small amount of additives (less than 10 wt%) and without annealing or seeding. Furthermore, the volume percentage of the elongated grains varies with the aluminum content. This processing strategy provides a simple way for producing SiC with distinctly different microstructures for the study of the relation between microstructures and mechanical properties.

3.3.2 Effect of Al wt% on β-to-α phase transformation

The volume percent of SiC polytypes is commonly quantified by XRD on the polished surfaces of bulk samples. The accuracy of this approach is limited by the complexity of the microstructures. First, the large plate-like grains prevent formation of a random grain orientation. This nonrandom orientation problem becomes more severe as the number of plate-like grain is reduced, as in 6ABC-SiC and 7ABC-SiC. Crushing the sintered materials into powder is not an effective solution to this problem because intergranular fracture is common, especially when aluminum content is less than 6wt%, as to be discussed later in the chapter. This will result in plate-like powders after crushing. Upon being pressed into a pellet, these plates will preferentially orient with the basal plane normal to the direction of pressure. In the current study, no preferential orientations of microstructure were produced due to hot-pressing. Therefore, as polished sample surfaces can actually provide a more representative XRD pattern.

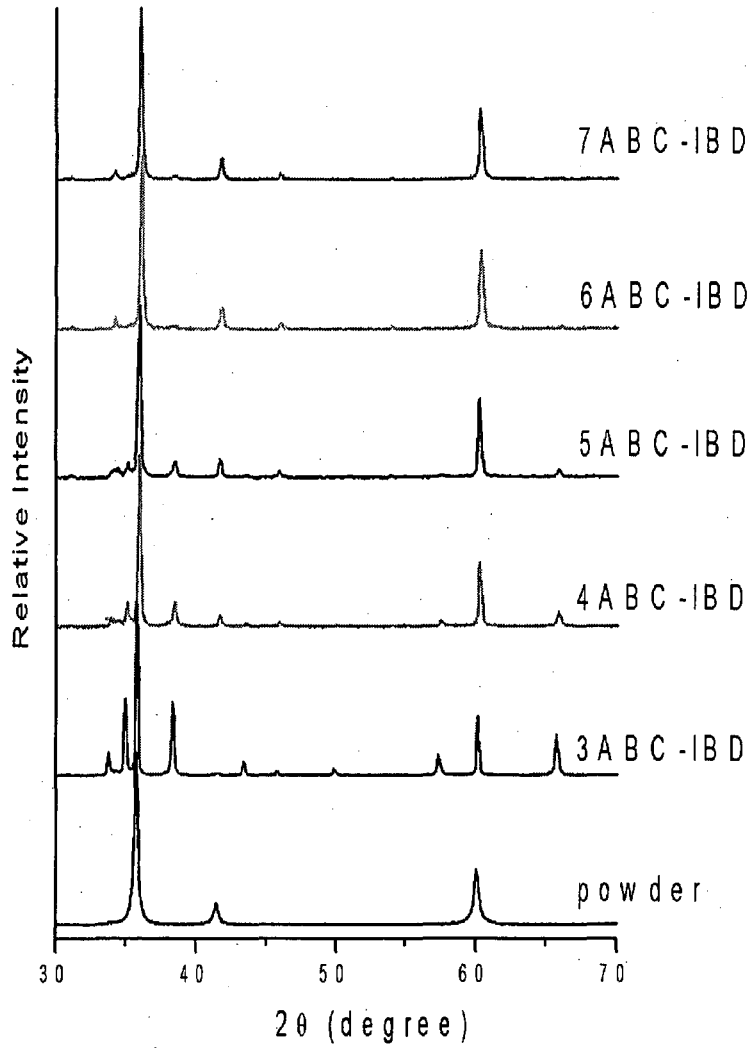

Figure 3-3. X-ray diffraction spectrum of the starting powder and hot-pressed ABC-SiC samples with different Al content.

Although quantitative XRD are limited in terms of accuracy due to the complex microstructure of SiC, it can still provide a statistically qualitative assessment of the phase transformation as a function of processing conditions. Figure 3-3 shows the XRD spectra from polished surfaces of the five materials, together with the spectrum of the starting powder. The starting powder only contains 3C. All of the five hot-pressed materials have more or less α-phase, depending on the amount of aluminum addition.

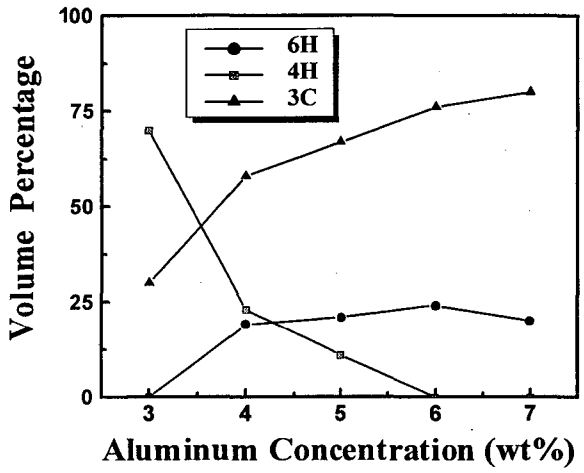

Figure 3-4: Volume fraction of polytypes in hot-pressed ABC-SiC materials as a function of Al wt%.

The major crystalline phase in 3ABC-SiC is 4H, and no 6H were detected. The polytype composition of 3ABC-SiC is in well agreement with the 3ABC-SiC produced by Cao[1]. Quite interestingly, 6H is the only detectable α-phase in 6ABC-SiC and 7ABC-SiC. Figure 3-4 shows the volume fractions of each SiC polytype, determined by Ruska's method[2], as a function of aluminum content. These results, together with data obtained by Cao[1], are also listed in Table 3-4. No other SiC polytypes (e.g., 15R) and peaks of other material (e.g., Al_2O_3) were evident in any composition that was processed in this study.

In a previous study[1], Cao compared the volume fractions of SiC polytypes in samples with 1 wt% and 3 wt% Al, both of which were hot-pressed at 1900°C for 1 hour. Samples with 3 wt% Al has 75 vol% 4H and 25 vol% 3C, whereas samples with 1 wt% Al did not transform at all (100 vol% 3C). Cao's result shows that aluminum promotes the β-to-α transformation. Many other researchers[13,14,15,16] reached similar conclusion regarding the effect of Al on the polytype transformation of SiC. However, in the current study the volume fraction of 3C increases and that of α-phase decreases as the Al wt% increases from 3 to 6. In another words, in the range of 3 wt% to 6 wt%, aluminum inhibits, instead of promotes, the transformation of 3C to 4H. The 6H and 15R polytypes are considered to be the intermediate products of 3C to 4H transformation[15]. Therefore,

the increase in 6H supports our finding that 3C to 4H transformation is retarded. 6ABC-SiC and 7ABC-SiC have almost the same volume fraction of 3C and 6H, which might indicate that further increasing the aluminum content will not substantially affects the β-to-α transformation. Combining the results of the current study and those of Cao's, we can say that aluminum enhances the β-to-α transformation when its concentration is less than 3 wt%, and inhibits the transformation when greater than 3 wt%.

Table 3-4: SiC polytypes of different hot-pressed SiC materials.

Materials	Al* (wt%)	3C# (vol%)	4H# (vol%)	6H# (vol%)
ABC-SiC C1[1]	1	100	0	0
ABC-SiC B3[1]	3	25	75	0
3ABC-SiC	3	30	70	0
4ABC-SiC	4	58	23	19
5ABC-SiC	5	67	11	21
6ABC-SiC	6	76	0	24
7ABC-SiC	7	80	0	20

* Weight percentage of aluminum in the starting powder.
\# Volume percentage calculated based on XRD using the method by Ruska *et al*[2].

In view of the limitations of quantitative XRD analysis, selective area diffraction (SAD) was carried out to determine the polytypes of different SiC grains. The elongated grains in 4ABC-SiC and 5ABC-SiC are either 6H or 4H. Most elongated grains in 7ABC-SiC are identified to be 6H and a few elongated 4H or 15R grains are also detected. The equiaxed grains in all the samples are 3C.

3.3.3 Correlation between Polytype Transformation, Microstructure Evolution and Additive Content

The elongated plate-like SiC grains are the result of polytype transformations, either from β to α, or from one type of α to another. The final microstructure, *i.e.* the size, shape, aspect ratio, and grain size distribution of SiC grains, depends on the nucleation and growth of grains of the new polytype. The fast growth of the plate-like grains requires an effective path for mass transport. This condition can usually be met in liquid phase sintered SiC. As a result, if the polytype transformation is favored, the resulting microstructure is uniform, with fine and plate-like grains; if the polytype transformation is not favored, the grains remain equiaxed. When only a small amount of grains can transform, the result is a bimodal grain size distribution: transformed, big plate-like grains, and untransformed small equiaxed grains. The microstructure-polytype content relation of ABC-SiC is in good agreement with this argument.

The polytype transformation is usually explained by the extension of stacking fault sequences[17,18,19] that can be either preexisting or produced by the incorporation of impurities. Many mechanisms have been proposed to explain the stabilization of the favored polytype, including the modification of bond strengths or lengths caused by substitutional impurities[20], generation and ordering of point defects[21], and lowering of the stacking fault energy by impurity or native defect interaction with the stacking faults of the parent polytype.[22] Both boron[23] and aluminum[24] can promote the β to α transformation in SiC when added separately to pure 3C SiC. The combined effect of boron and aluminum doping on the polytype transformation is even more dramatic because of the enhanced mass transport through liquid phase in Al-doped SiC. However,

in our Al, B, and C doped SiC, a higher Al content inhibits the 3C to 4H transformation. This indicates that the driving force for the nucleation and growth of stacking faults in SiC lattice is reduced.

In the SiC lattice, boron occupies both Si and C sites and leads to lattice contraction, whereas aluminum substitutes Si and causes lattice expansion[16]. If local lattice strain caused by the impurities is the primary driving force for the nucleation and extension of stacking faults in SiC, then at some particular Al/B ratio, Al and B may cancel out each other's effect on the lattice deformation. Hence a slowdown of the β-to-α transition could be observed. The Al/B ratio in the SiC lattice can be affected by many processing conditions that can change the solubility of the Al and/or B in SiC, such as additive content, temperature, pressure, etc. In the ABC-SiC samples, it seems that the critical Al/B ratio in the SiC lattice is reached after the overall Al content exceeds 6wt%.

A direct prove/disprove of this assertion may be a series of experiments that measure the change of lattice constant of SiC and stacking fault density as function of Al/B ratio in the SiC lattice. This is out side of the scope of the current study. Instead, the proposed model is tested indirectly. If the above assumption is true, then any process than can change the Al/B ratio in the SiC lattice will result in different microstructures and polytype contents of SiC. Increasing or reducing the B additive amount is an obvious approach. A variation in the carbon content may also affect the polytype transformation and the microstructure since it will indirectly change the B content in the system. It is well known that carbon is required for the sintering of B doped SiC because carbon reacts with and removes the oxides[3,25] such as Al_2O_3 and SiO_2, which always exist on the metallic Al or SiC particles if the powders are handled in air. In the absence of carbon,

these oxides can react with B, produce gaseous B_2O_3, and remove B from the system. Furthermore, Al and C can form stable compound Al_3C_4. All these reactions change the chemical environment surrounding the SiC grains and affect the Al/B ratio in the SiC lattice. Therefore, a higher carbon content is expected to increase the Al/B ratio in SiC lattice.

To test this assumption, samples with same nominal Al content (6wt%) and different B and/or C additive amount were hot-pressed and characterized. The additive composition and polytype content of SiC after hot-pressing are summarized in Table 3-5 and the comparison of the microstructures are shown in Figure 3-5. The two boron rich (0.9wt%) samples have almost completely transformed to 4H. The 0.3wt% increase of the boron content dramatically enhances the 3C-to-4H transformation. The resulting microstructures are uniformly elongated plate-like grains, which is a common feature in well transformed SiC ceramics.

Table 3-5. Effect of Boron and Carbon Additive Compositions on the Polytype Content of Hot-pressed SiC

Materials*	B (wt%)	C (wt%)	3C (vol%)	4H (vol%)	6H (vol%)
6A6B2C#	0.6	2	76	0	24
6A6B3C	0.6	3	36	37	27
6A9B2C	0.9	2	0	97	3
6A9B3C	0.9	3	0	94	6

* All samples contain 6wt% aluminum and were processed under the same condition as described in Section 3.2.1.
# This is the 6ABC-SiC in Table 3-2.

Increasing carbon content is also helpful for the β-to-α transformation, although the effect is much less dramatic than that of boron. Comparing to 6A6B2C, sample 6A6B3C has a higher α content, which results in the apparent bimodal grain size

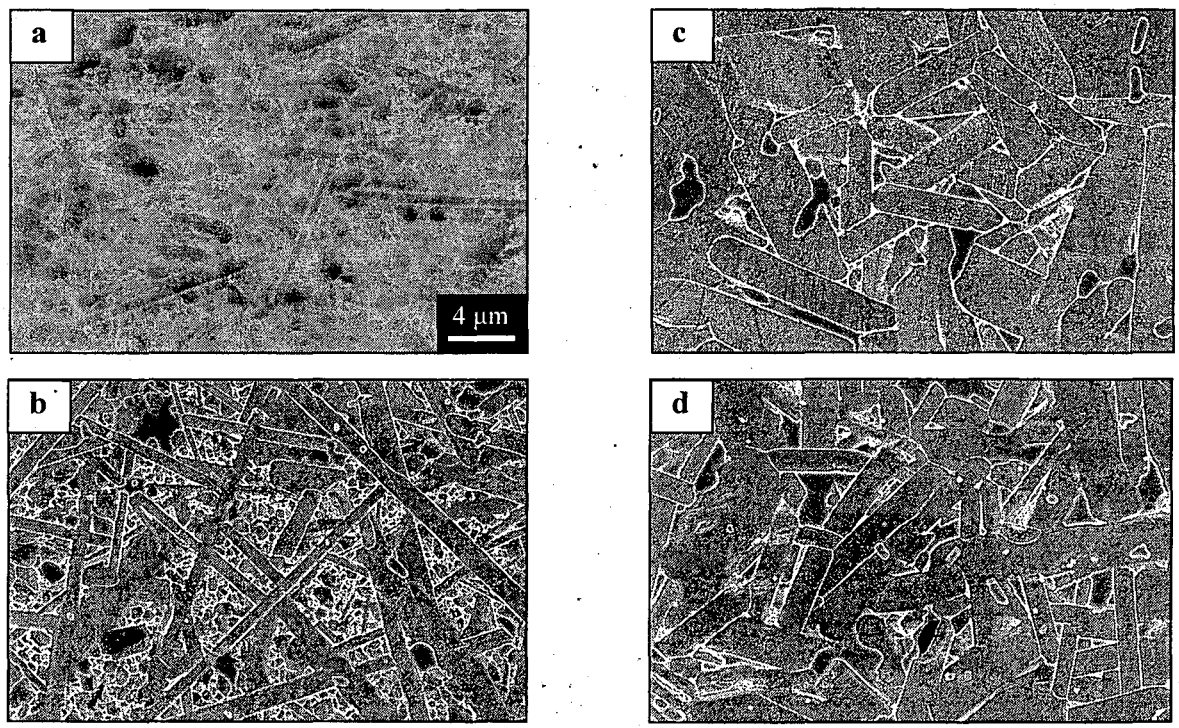

Figure 3-5. Microstructure of hot-pressed SiC with 6wt% Al but different B and C addition content. (a) 6A6B2C, (b) 6A6B3C, (c) 6A9B2C, (d) 6A9B3C.

distribution and much higher volume percent of elongated plate-like grains. Note that carbon also affects the grain size of the two boron rich samples: 6A9B3C has an apparently smaller grain size than 6A9B2C. This indicates a higher density of α-polytype nuclei in the carbon rich sample 6A9B3C.

Although the above experiment cannot rigorously prove our Al/B ratio model, our results so far match well with the inferences of the model. In summary, changing the additive content of ABC-SiC results in a change of the environment that SiC grains are in. This causes the impurity Al/B ratio inside SiC grains to vary. As a consequence, the polytype transformation and grain morphology can be controlled by simply choosing the amount of Al, B and C additives.

3.3.4 Effect of the Al Content on Grain Boundary Films

Collaborative TEM work Zhang on 3, 4, 5, and 7ABC-SiC samples was carried out with Dr. X.F. to study the grain boundary films. HRTEM found that grain boundary films change from amorphous to crystalline as the overall Al content of the sample increases. Figure 3-6 shows the HRTEM images of various grain boundaries in 3, 5 and 7ABC-SiC. The grain boundaries in 3ABC-SiC are amorphous, which is common in liquid phase sintered SiC. Amorphous, crystallized, and partially crystallized grain boundaries exist in 4ABC-SiC and 5ABC-SiC, the amount of crystallized grain

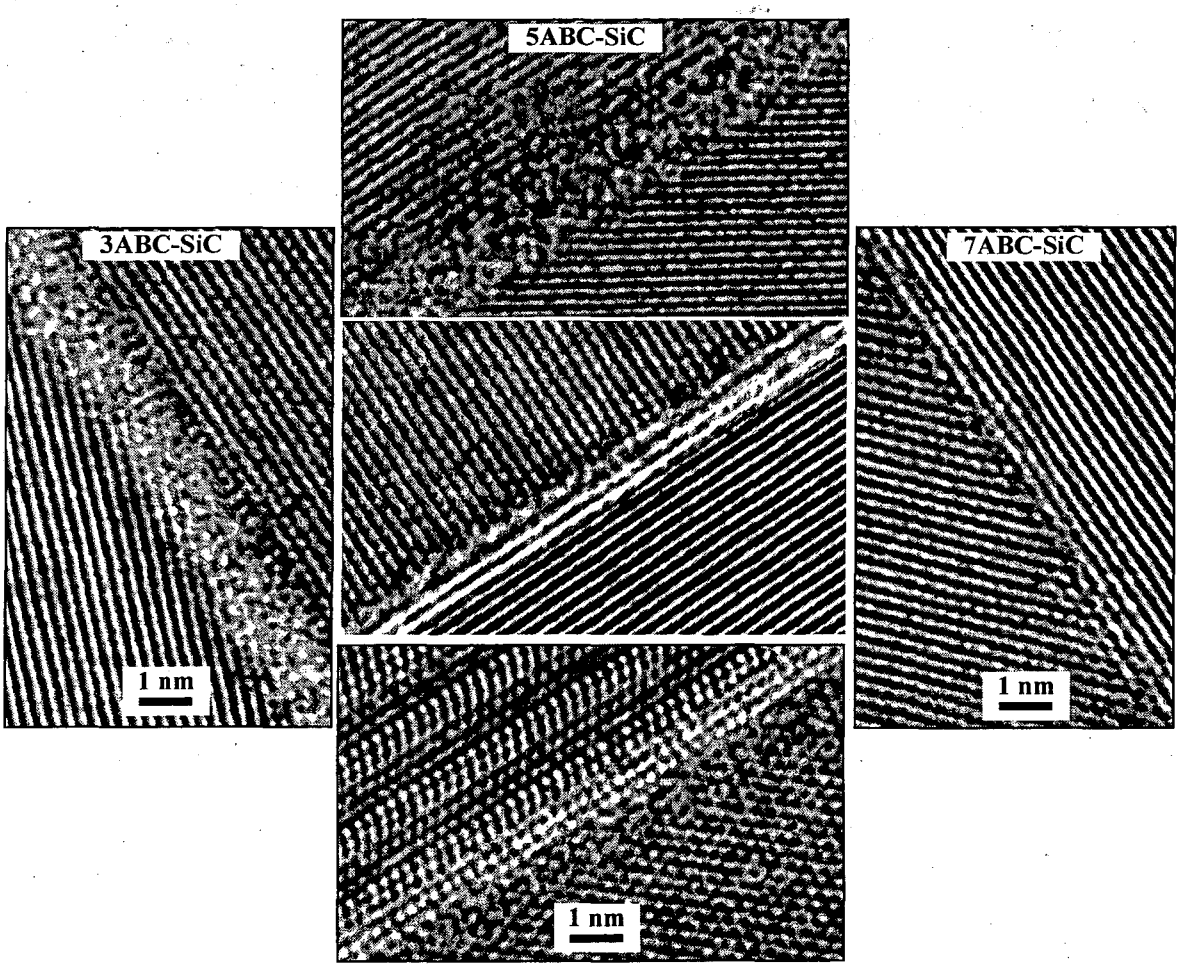

Figure 3-6: High resolution TEM micrographes: a comparison of the grain boundaries in the hot-pressed SiC materials with different Al content. Courtesy of Dr. X. F. Zhang.

boundaries is minimal, however. In 7ABC-SiC, only crystallized grain boundaries were detected.

It has been found by Zhang et al.[26] that the Al rich amorphous grain boundary films in 3ABC-SiC crystallize during a post hot-press heat treatment. If one defines the aluminum excess as the difference between the area density of Al at the grain boundary and the area density of Al in SiC grains, the Al excess increases after grain boundary films crystallized. This is possibly caused by the diffusion of Al from SiC grains or triple points to the grain boundaries. Since the two approach, i.e. heat treatment and increasing the overall aluminum content in the sample, have similar effects on the evolution of grain boundary films, it is plausible that the crystalline grain boundary films in this study have higher aluminum content than the amorphous grain boundary films. However, quantitative EDS did not show an apparent difference in the Al excess of the amorphous and crystalline grain boundary films in this study. Furthermore, the Al concentration in SiC grains are similar: 1.3 wt% for 3ABC-SiC, and 1.5~1.7 wt% for 4 to 7ABC-SiC.

The almost invariant Al content at the grain boundaries suggests changes in the contents of other elements such as B, C, and O in the grain boundaries. A decrease in B, C, or O content is equivalent to the increase of Al/B, Al/C, or Al/O ratio at the grain boundaries. According to the phase diagrams[27,28] shown in Figure 3-7, when the local composition varies slightly, crystalline grain boundary films or high viscosity liquid may form. This argument can be proved or negated if the contents of B, C, and O at the grain boundaries are known. However, the direct EDS quantification is practically impossible due to the factors such as the small quantity of these elements, contamination during the TEM sample preparation, and strong absorption of x-ray signals.

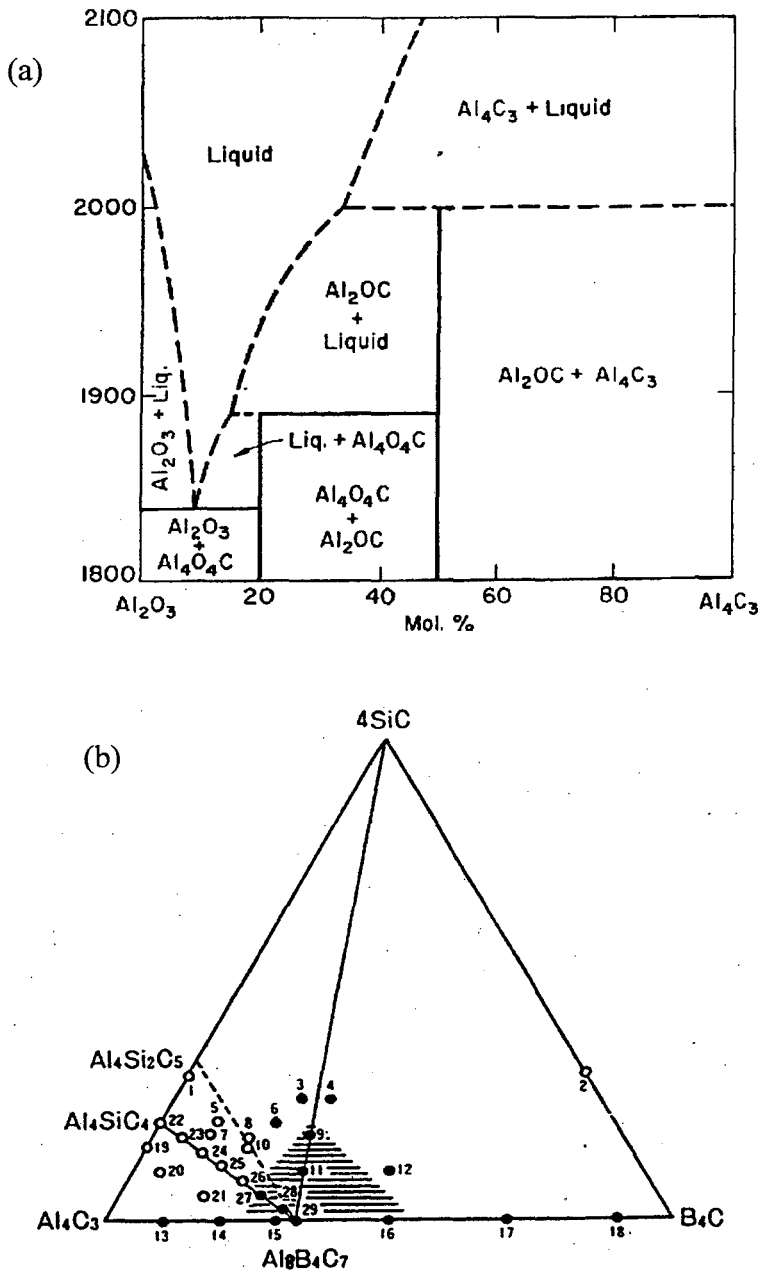

Figure 3-7: (a) Phase diagram of Al_3O_2-Al_4C_3 system.[27]
(b) Phase relationships for the SiC-B_4C-Al_4C_3 system at 1800°C.
The shaded area is the region where a liquid was formed at 1800°C.[28]

3.3.5 Secondary Phases and Inclusions

Aluminum can substitute for Si in SiC and form substitutional solid solutions. The solubility limit of Al in SiC was reported to be1.0wt% at 2200°C[16]. The amount of

aluminum in our SiC materials is well beyond this solubility limit. Besides forming Al rich grain boundaries, Al also exists in triple points and secondary phases[29]. TEM study has found that Al_4C_3 and Al-C-O grains are attached to the elongated grains in 7ABC-SiC. Pure metallic Al was also detected in 7ABC-SiC, which exists as networks in the matrix of SiC grains, as shown in Figure 3-8. This free Al may be detrimental to the high temperature mechanical properties of SiC. Pure Al was not detected in 3, 4 and 5 ABC-SiC.

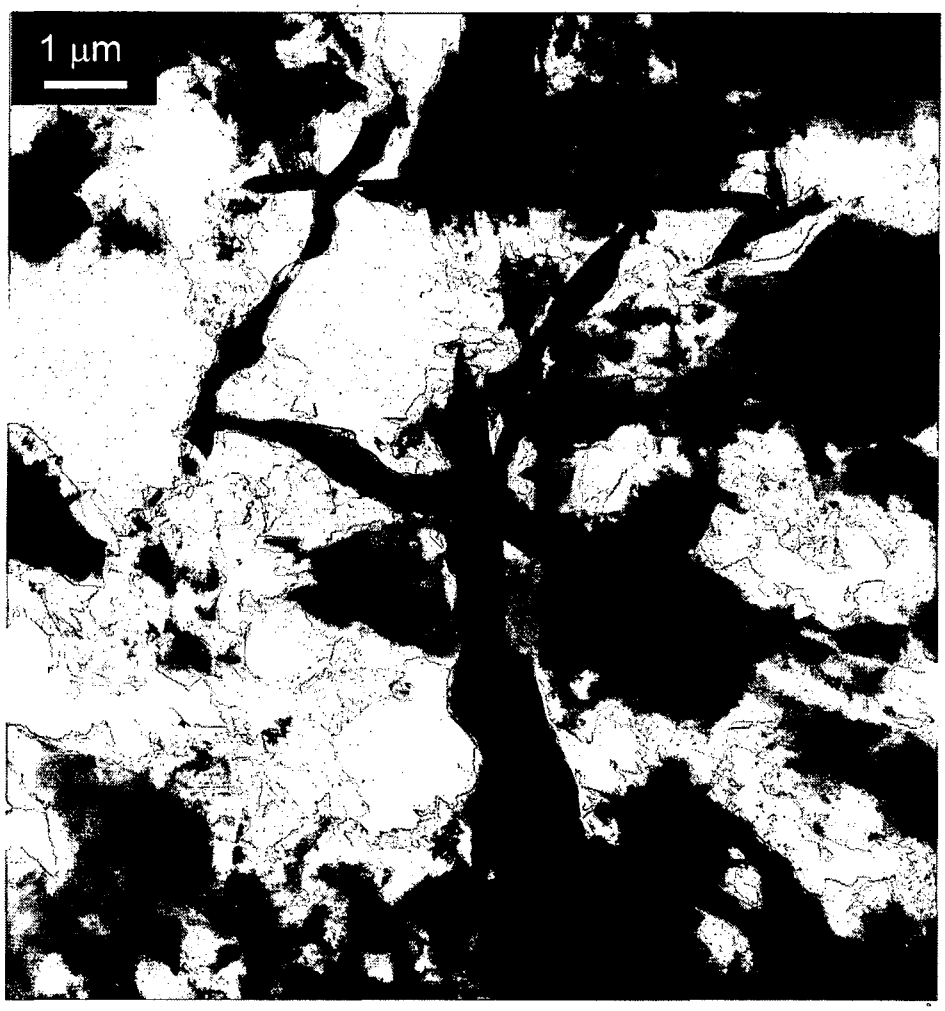

Figure 3-8: TEM micrograph of 7ABC-SiC. The dark steaks is the residual aluminum metal. (Courtesy of Dr. X.F. Zhang)

The additives not only form grain boundary phases and secondary phases but are also present as inclusions inside big plate-like silicon carbide grains. Figure 3-9 shows an Al-C inclusion in a 4H-SiC grain. EDS spectra collected from three different spots *i.e.*

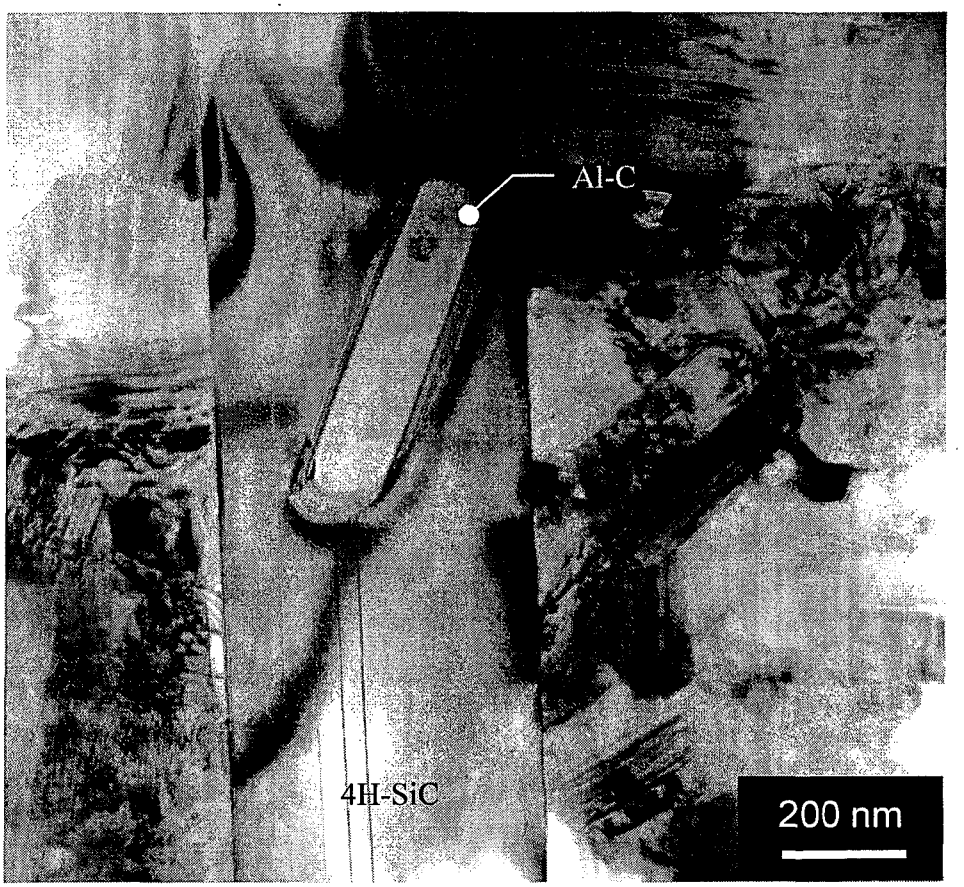

Figure 3-9: TEM micrograph of an Al-C inclusion in a 4H-SiC grain. Material: 7ABC-SiC. (Courtesy of Dr.X.F. Zhang)

inclusion inside the grain, SiC grain and secondary phase were compared in Figure 3-10. Both the inclusion and the secondary phase show strong Al peaks. In contrast, almost no Al was detected in the SiC grains. It is interesting to note that the big grain in Figure 3-10 is a plate-like grain that is almost parallel to the polished surface. This grain is interlocked with many other elongated grains.

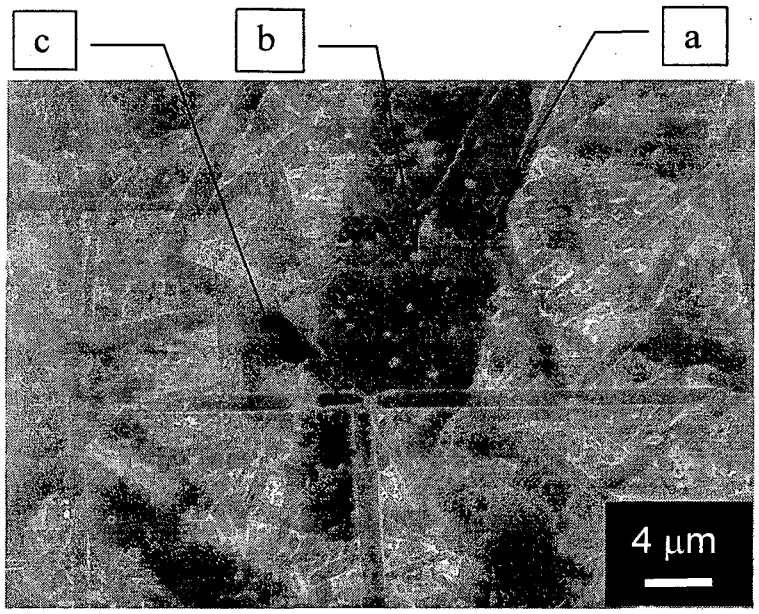

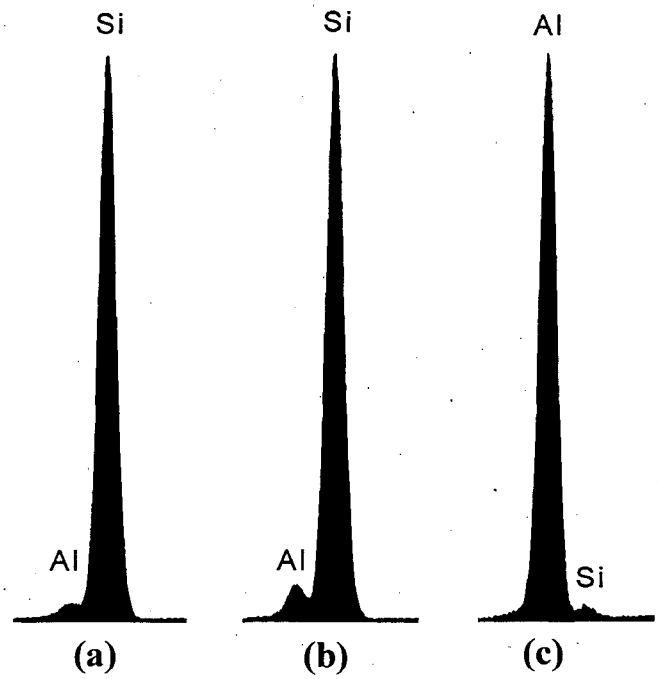

Figure 3-10:Energy dispersive spectrometry (EDS) of 5ABC-SiC, (a) .SiC grain, (b) inclusion, and (c) secondary phase. The big plate-like grain lies almost parallel to the polished surface. Note also the many interlocks between this grain and others.

3.3.6 Effect of Starting Powders

Table 3-6: Comparison of the properties of starting powders.

	IBIDEN BETARUNDUM grade ultra-fine	H.C. STARCK SiC grade B 20
Free C (wt %)	1.03	0.04*
Free SiO_2 (wt %)	0.47	not available
O (wt %)	not available	1.20
Fe (ppm)	178	280
Al (ppm)	210	110
Ca(ppm)	21	12
Average diameter (μm)	0.30	0.52
Specific Surface Area (m^2/g)	20.5	20.5

* Calculated according to the 30.00% C in the analytical report of the powder.

It is necessary to discuss the similarity and difference of the SiC with an aluminum concentration gradient (Chapter 2) and those with homogeneous aluminum distribution (this Chapter). First, the grain morphology of 3ABC-SiC resembles that of region *b* in Figure 2-5. Second, a higher aluminum content facilitates the preferential growth of some SiC grain and results in enhanced aspect ratio and a bimodal grain size distribution. However, a microstructure similar to the one shown in Figure 2-5 *a* is not evident in any of the five SiC materials with homogeneous aluminum distribution. The smaller grains are equiaxed in the four materials 4, 5, 6 and 7 ABC-SiC. In contrast, both the larger and the smaller grains shown in Figure 2-5 *a* are elongated. This discrepancy is possibly due to the difference in the starting powder. Although both powders are very pure 3C as shown in Figure 3-11, slight differences do exist in the impurities of the powders. Table 3-6 lists the specification of the two SiC powders. Since the grain

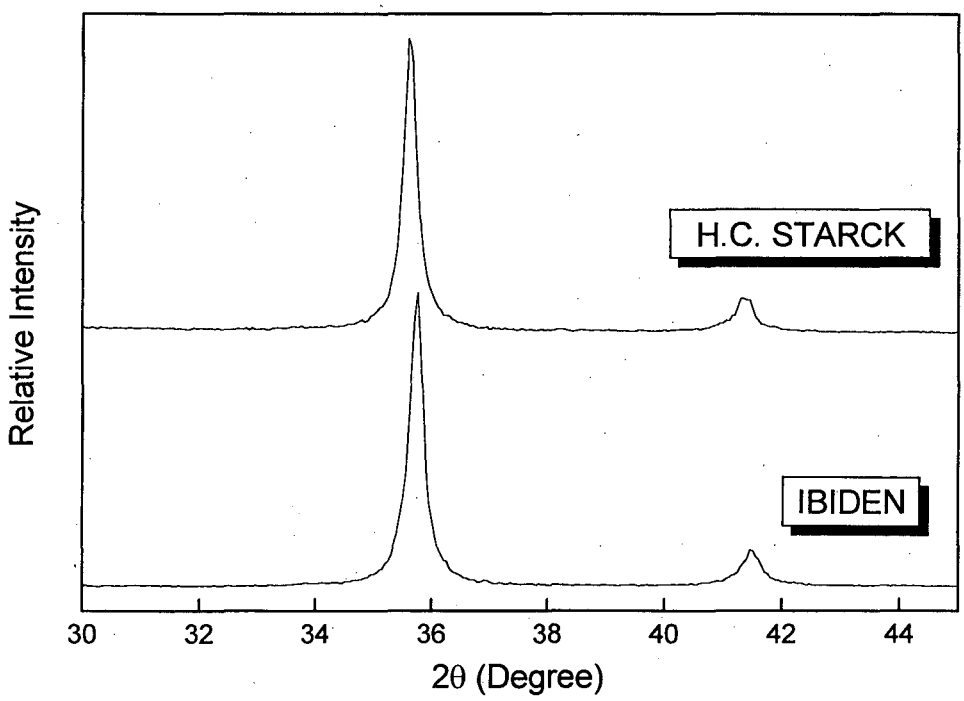

Figure 3-11: X-ray diffraction spectrum of the two SiC powders. Both of are pure 3C. No apparent differences in the spectra are observed.

boundary property is very sensitive to the chemistry, it is not surprising to find the difference in the microstructure when using different starting powders. Other properties of the powder such as the particle size, size distribution and stacking fault density may also have effects on the microstructure.

3.3.7 Effect of Microstructure on Mechanical Properties

The mechanical properties of SiC are directly related to its microstructures. As shown above, the materials with different aluminum content have different grain morphology, grain boundary and polytypical composition. This implies varied mechanical properties as the aluminum content changes. Figure 3-12 plots the variation of the four-point bending fracture strength as a function of the aluminum content. The

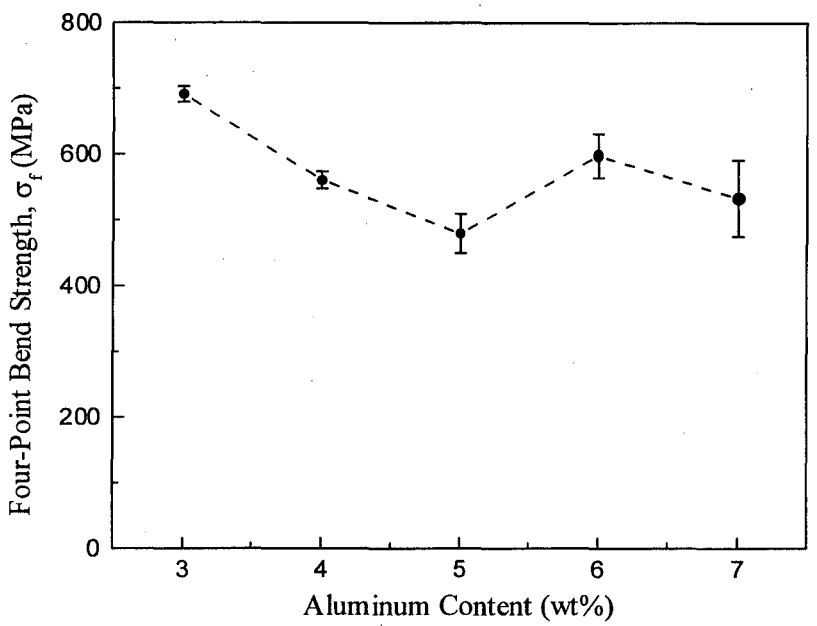

Figure 3-12: Four-point bend strength as a function of the aluminum concentration of the hot-pressed ABC-SiC ceramics.

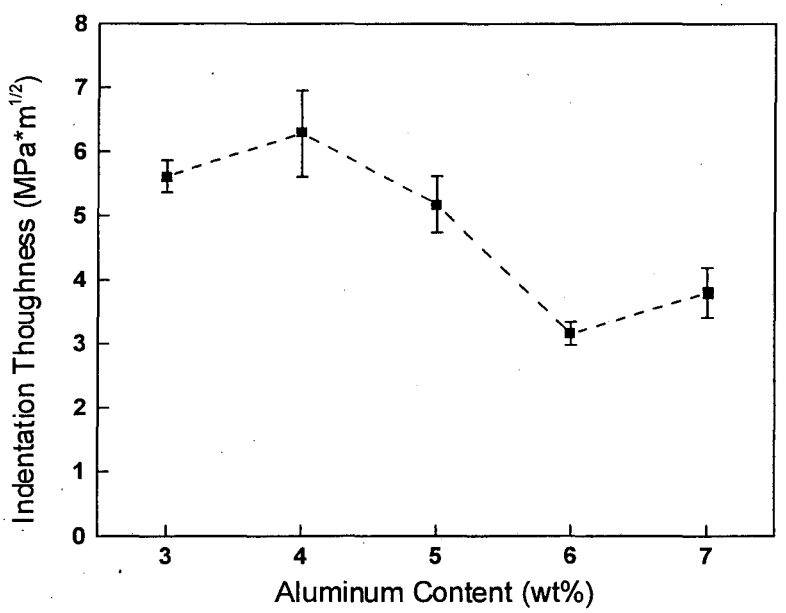

Figure 3-13: Indentation toughness as a function of the aluminum concentration of the hot-pressed ABC-SiC ceramics.

fracture strength changes in an opposite way as the grain length. As expected, a large grain size is deleterious to the fracture strength. 3ABC-SiC has the highest fracture

strength, which is more than 40% higher than that of 5ABC-SiC. The large deviation of the strength of 6ABC-SiC and 7ABC-SiC is due to the poor toughness of the two materials.

Figure 3-13 shows the variation of indentation toughness of the five materials as a function of the Al wt%. The toughness first increases and then decays as the aluminum content increasing and peaks at 4ABC-SiC (6.4MPa√m). Several factors that affect the toughness are discussed below.

As mentioned before, the majority grains in 3, 4, and 5 ABC-SiC are elongated plate-like grains, whereas the microstructures of 6 and 7 ABC-SiC are dominated by fine equiaxed grains. 3, 4 and 5 ABC-SiC have toughness above 5 $MPa \cdot m^{1/2}$; and the toughness of 6 and 7ABC-SiC are less than 4 $MPa \cdot m^{1/2}$. The crack profiles in Figure 3-14 *a* to *c* show tortuous paths and many bridging sites. In contrast, the cracks in Figure 3-14 *d* and *e* are straight, showing no significant grain bridging. Even though 6 and7 ABC-SiC have the highest aspect ratios among all the materials being investigated in this study, the volume fraction of elongated grains is too small to contribute to improve the toughness.

It is commonly accepted that the toughness of SiC increases with the aspect ratio of elongated plate-like grains. However, this conclusion was drawn from SiC with the highest aspect ratios of about 10. In the current study, the aspect ratio of elongated grains varies from about 5 to above 30, which provides a much broader range to investigate the relation between the aspect ratio and the fracture toughness. Since the number of elongated grains in 6 and 7 ABC-SiC is too low, the two materials are similar to pure fine grain, equiaxed SiC, and it is more meaningful to restrict our discussion on the role of

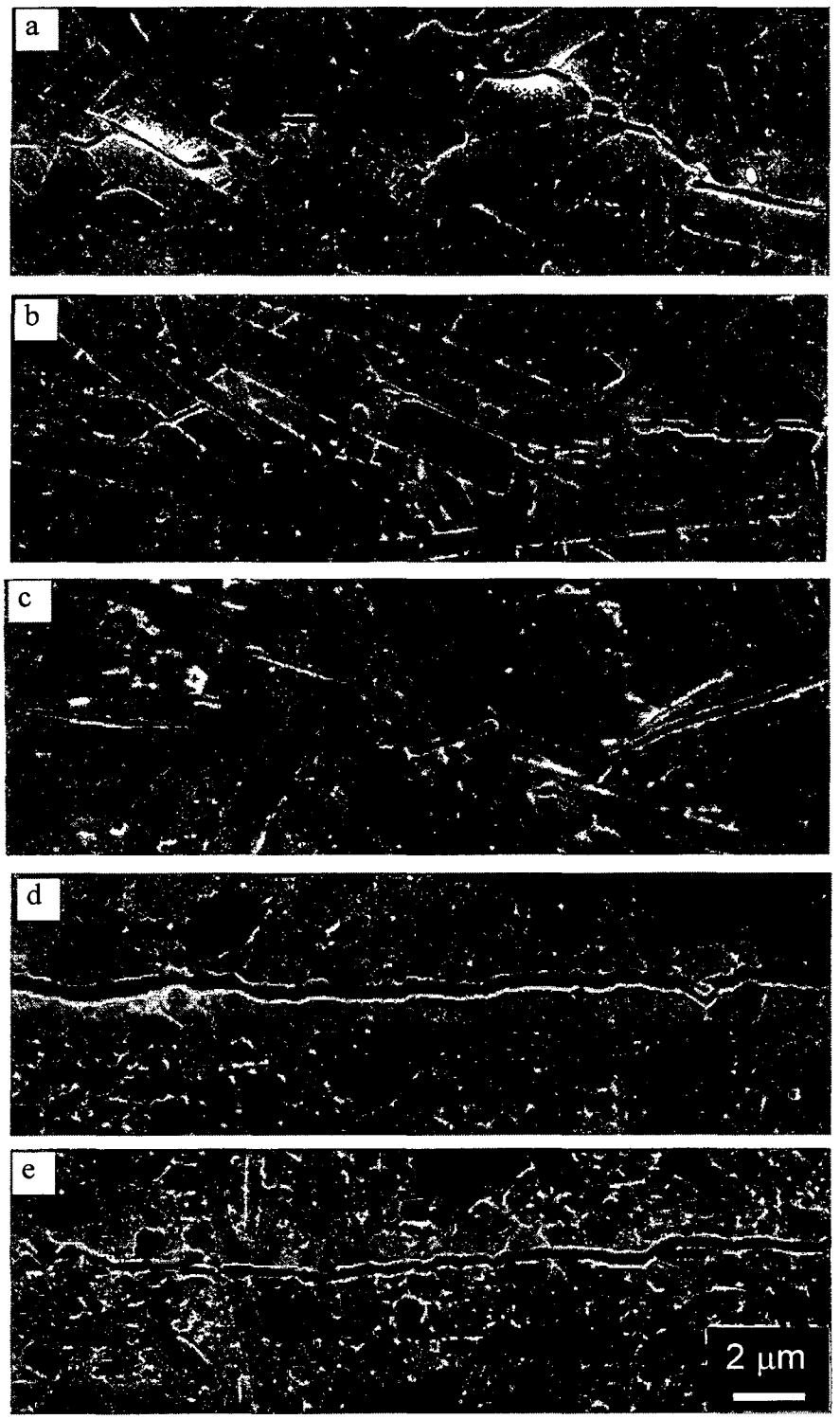

Figure 3-13: Crack profiles of hot-pressed ABC-SiC.
(a) through (e): 3,4,5,6, and 7ABC-SiC.

aspect ratio to 3, 4 and 5 ABC-SiC. Both the grain length and the aspect ratio of the three

materials increase with the increasing of aluminum content. The toughness value peaks at 4ABC-SiC, which most likely indicates that there is an optimal aspect ratio, or grain length, or both, corresponding to the highest toughness.

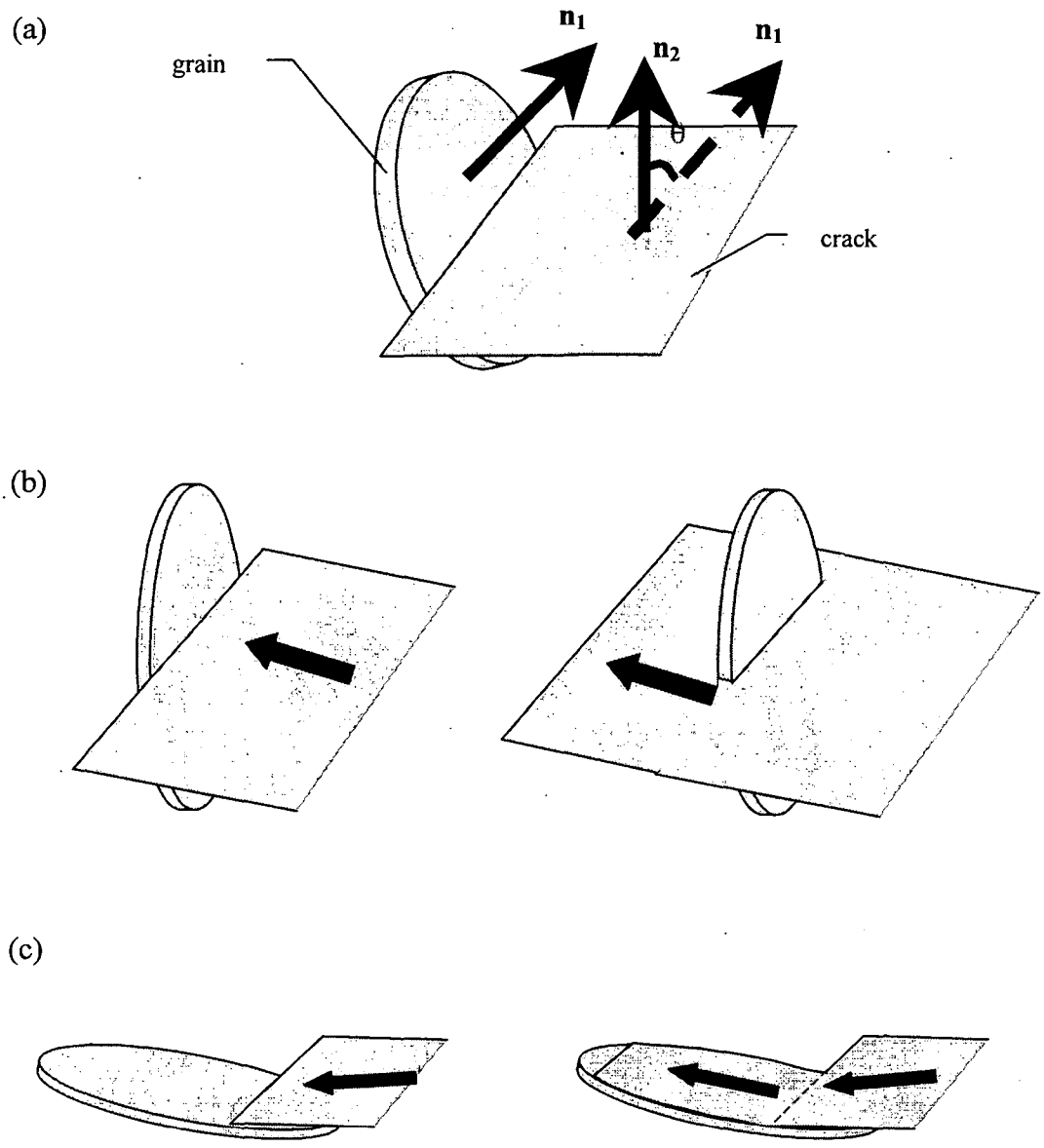

Figure 3-15: Dependence of the crack path on the orientation between the crac plane and plate-like grain. (a) Incident angle θ is defined as the angle between th normal of the plate-like grain $\mathbf{n}_1$ and the crack normal $\mathbf{n}_2$. (b) $\theta \approx 90°$, fracture of th grain, and (c) $\theta \approx 0°$, interfacial debonding. The arrows on the crack plane indicat the crack propagation direction.

As shown is Figure 3-14, the propagating of cracks become more sensitive to the orientation of elongated grains as the aspect ratio and grain length increase. Figure 3-15 illustrates the role of the orientation of elongated plate-like grains in toughened SiC. When a grain lies almost normal to the crack (angle of incident $\theta \approx 90°$), the crack passes right through it. When a crack approaches a plate shaped grain at a very small incident angle ($\theta \approx 0°$), interfacial debonding occurs and crack propagates easily along the surface (usually >10 μm in diameter) of the grains. Neither of the two cases provides effective bridging or crack deflection. Most of the grains that act as bridging sites or cause a tortuous crack path are those with intermediate incident angles. The low fracture toughness of 6 and 7ABC-SiC can be further explained by the small number of elongated grains that lie within the effective range of the incident angle per unit crack face area. The nature of the grain boundaries then is not a dominant factor determining the fracture mode.

Fractographes of the five materials are shown in Figure 3-16 *a* through *e*. The fracture surface of 3ABC-SiC is dominated by intergranular fracture. 4ABC-SiC shows a bigger fraction of transgranular fracture resulting from that highly elongated grains fracture at interlocks. In addition, a few small facets can be observed. These facets are mostly the surfaces of big plate-like grains that lie almost parallel to the fracture surface. Both the fracture surfaces of 3ABC-SiC and 4ABC-SiC are rough, showing numerous peaks and valleys. This indicates a high degree of crack deflection, grain bridging and pull out. The fracture surface of 5ABC-SiC is still rough, but shows more facets, whose size is bigger than those in 4ABC-SiC. This is consistent with the somewhat smaller toughness of 5ABC-SiC compared to that of 3 and 4ABC-SiC. On some facets, some

imprints of other elongated grains can be seen. This again shows that many elongated grains fractures at the interlock. The fine equiaxed grains fracture intergranularly. The fracture surfaces of 6ABC-SiC and 7ABC-SiC are relative flat, corresponding to the smaller fracture toughness than 3 to 5ABC-SiC. The fracture mode of the plate-like grains depends on the incident angle. Some big facets on the fracture surfaces resulted from either the debonding along the side of large plate-like grains or the transgranular fracture of the big grains.

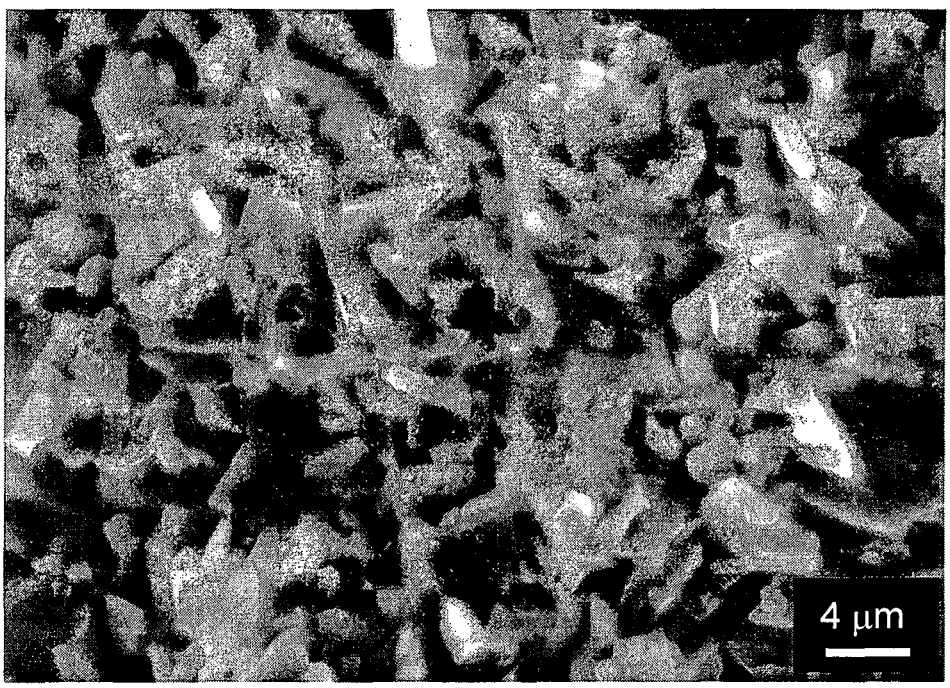

Figure 3-16 (a) 3ABC-SiC

Figure 3-16 (b) 4ABC-SiC

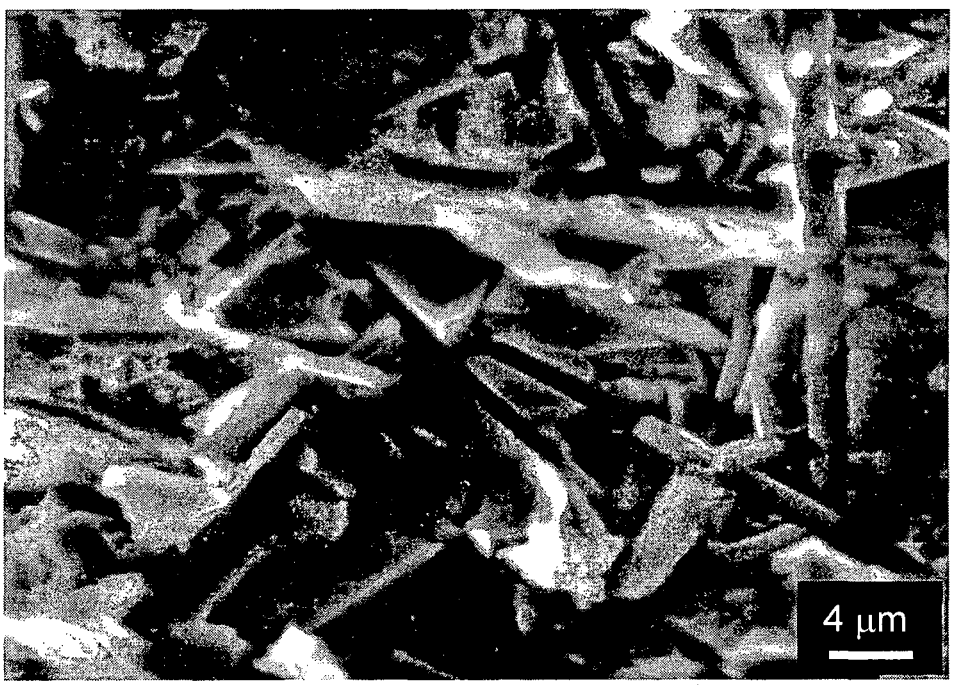

Figure 3-16 (c) 5ABC-SiC

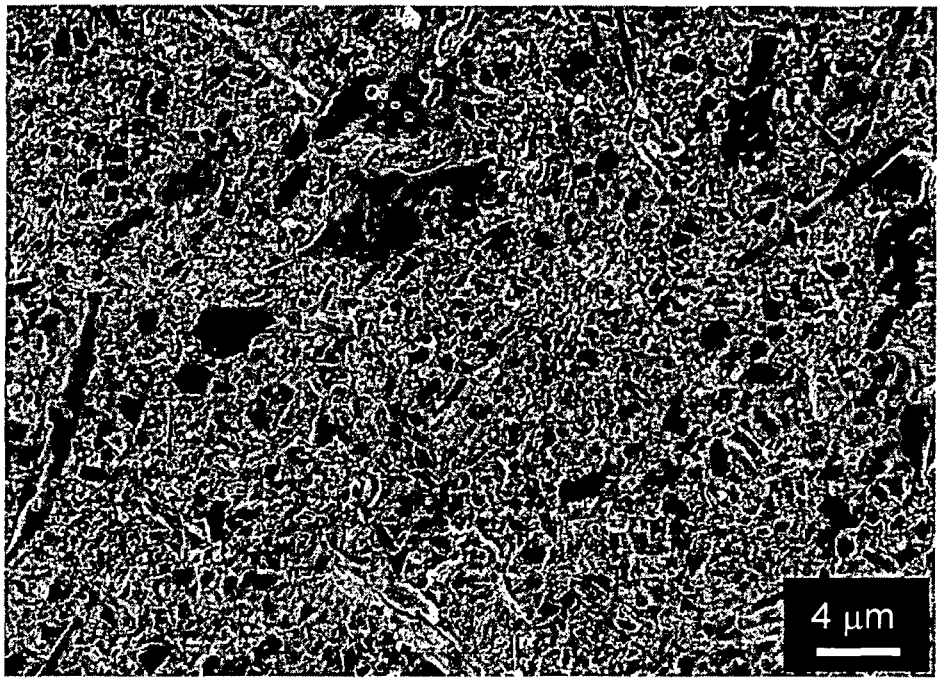

Figure 3-16 (d) 6ABC-SiC

Figure 3-16 (e) 7ABC-SiC

Figure 3-16: Fractographs of ABC-SiC ceramics with different Al content.

3.4 Conclusions

The microstructure and room temperature mechanical properties of hot-pressed silicon carbides with 3wt% to 7 wt% aluminum addition have been investigated. It was found that a small variation of the aluminum content can drastically change the microstructure and hence the mechanical properties of silicon carbide. Grain boundaries of as hot-pressed SiC change from amorphous to crystalline as the aluminum content increases, which is presumably due to the change of the local chemical composition. The change of the nature of the grain boundaries results in the retarded β-to-α transformation. As a consequence, when the aluminum content varies from 3wt% to 7wt%, the elongated plate-like grains change as follows: the aspect ratio increases about 6 times, the volume fraction decreases, the length increases first and then decreases with the peak at 5wt% aluminum addition.

The effect of the microstructure on the room temperature mechanical properties was investigated. Silicon carbide with less than 5wt% aluminum addition have high fracture toughness. The fracture toughness increases with the aspect ratio but decreases as the volume fraction of elongated grains decreases. The fracture mode of elongated grains depends on their orientation to the crack path. Fracture strength decreases with the increasing of grain size. 4ABC-SiC shows the highest fracture toughness (6.3MPa√m) as well as high fracture strength (561MPa).

3.5 References

[1] J. Cao, "*In Situ* Toughened SiC Ceramics with Al-B-C Additions and Oxide-Coated SiC Platelet/SiC Composites," Ph.D. Thesis, University of California, Berkeley, pp. 22, (1996).

[2] J. Ruska, L.J. Gauckler, J.L. Lorenz, and H.U. Rexer, "The Quantitative Calcualtion of SiC Polytypes from Measurements of X-ray Diffraction Peak Intensities," *J. Mater. Sci.*, **14** [8] 2013-17 (1979).

[3] S. Prochazka, "The Role of Boron and Carbon in Sintering of Silicon Carbide," Special Ceramics, Vol. 6, pp. 171-181 (1975).

[4] D.H. Stutz, S. Prochazka, and J. Lorenz, "Sintering and Microstructure Formation of β-Silicon Carbide," *J. Am. Ceram. Soc.*, **68** [9] 479-82 (1985).

[5] A.H Heuer, G.A.Fryburg, L.U. Ogbuji, T.E. Mitchell, and S. Shinozaki, "β-->α Transformation in Polycrystalline SiC: I, Microstructural Aspects," *J. Am. Ceram. Soc.*, **61** [9-10] 406-12 (1978).

[6] S.S. Shinozaki, R.M. Williams, B.N. Juterbock, W.T. Donlon, J. Hangas and C.R. Peters, "Microstructure Developments in Pressureless-Sintered β-SiC Materials with Al, B, and C Additions," *J. Am. Ceram. Soc.*, **64** [10] 1389-93 (1985).

[7] P.F. Becher, "Microstructural Design of Toughened Ceramics," *J. Am. Ceram. Soc.*, **74** [2] 255-69 (1991).

[8] Y-W. Kim, M.Mitomo, H, Emoto, and J-G. Lee, "Effect of Initial α-Phase Content on Microstructure and Mechanical Properties of Sintered Silicon Carbide," *J. Am. Ceram. Soc.*, **81** [12] 3136-40 (1998).

[9] P.F. Becher, E.Y. Sun, K.P.Plucknett, K.B. Alexander, C-H Hsueh, H-T. Lin, S.B. Waters, and C.G. Westmoreland, "Microstructural Design of Silicon Nitride with Improved Fracture Toughness: I, Effects of Grain Shape and Size," *J. Am. Ceram. Soc.*, **81** [11] 2821-30 (1998).

[10] E.Y.Sun, P.F. Becher, K.P. Plucknett, C-H Hsueh, K.B. Alexander, , S.B. Waters, K. Hirao, and M.E. Brito, " Microstructural Design of Silicon Nitride with Improved Fracture Toughness: II, Effects of Yttria and Alumina Additives," *J. Am. Ceram. Soc.*, **81** [11] 2831-40 (1998).

[11] N. P. Padture and B.R. Lawn, "Toughness Properties of a Silicon Carbide with an *In Situ* Induced Heterogeneous Grain Structure," *J. Am. Ceram. Soc.*, **77**[10] 2518-22 (1994).

[12] J-Y Kim, Y-W Kim, M. Mitomo, G-D Zhan, and J-G Lee, "Microstructure and mechanical Properties of α-Silicon Carbide Sintered with Yttrium-Aluminum Garnet and Silica," *J. Am. Ceram. Soc.*, **82**[2] 441-44 (1999).

[13] W, Bocker, R.H. Landfermann, and H. Hausner, "Sintering of Alpha Silicon Carbide Powder with Additions of Aluminum," *Powder Met. Intl.* **11**(2), 83-85 (1979).

[14] R. Hamminger, G. Grathwohl, and F. Thummler, "Microanalytical Investigations of Sintered SiC; Part1, Bulk Materials and Inclusions," *J. Mat. Sci.*, **18** 353-64 (1983).

[15] R.M. Williams, B.N. Juterbock, S.S. Shinozaki, C.R. Peters, and T.J. Whalen, "Effects of Sintering Temperatures on the Physical and Crystallographic Properties of β-SiC," *J. Am. Ceram. Soc.*, **64** [10] 1385-89 (1985).

[16] Y. Tajima and W.D. Kingery, "Solid Solubility of Aluminum and Boron in Silicon Carbide," *Comm. Am. Ceram. Soc.*, **65** [2] C27-29 (1982).

[17] H. Jagodzinski, *Acta Cryst.*, **7**, 300 (1954).

[18] D. Pandey and P. Krishna, Porc. 3rd Int. Conf. on SiC, Florida, Ed. by R.C. Marshall, J.W. Faust and C.E. Ryan (1973) pp. 198-206.

[19] N.W. Jepps and T.F Page, *J. Cryst. Growth Characterization*, **7**, 259-307 (1983).

[20] P. Bak, S. Coppersmith, Y.Shapir, S.Fishman and J. Yeomans, *J. Phys. C*, **18** (1985) 3991.

[21] A. Krol, M.J. Kozielski and W. Nazarevicz, *Bull. Minearl.* **106** (1986) 81.

[22] A.N. Pilyankevich, V.F. Britun and G.S.Oleynik, *J. Mater. Sci.*, **25** (1990) 3517.

[23] J. Pezoldt, "Are polytype transitions possible during boron diffusion?" *Materials Sci. Engi.* **B29** (1995) 99-104.

[24] W-S. Seo, C.H. Pai, K. Koumoto, and H. Yanagida, "Roles of Stacking Faults in the Phase Transformation of SiC," *J. Ceram. Soc. Jp.* **100** [3] 227-232 (1992).

[25] W.J. Clegg, "Role of carbon in the Sintering of Boron-doped Silicon Carbide," *J. Am. Ceram. Soc.*, **83** [5] 1039-43 (2000).

[26] X.-F. Zhang, M.E. Sixta, and L.C. De Jonghe, "Grain-Boundary Evolution in Hot-Pressed ABC-SiC," *J. Am. Ceram. Soc.*, **83** [11] 2813-20 (2000).

[27] L.M. Foster, G. Long, and M.S. Hunter, "Reactions between Aluminum Oxide and Carbon -- The Al_2O_3 -- Al_4C_3 Phase Diagram," *J. Am. Ceram. Soc.*, **39** [1] 1-11 (1956).

[28] Y. Inomata, H. Tanaka, Z. Inoue, and H. Kawabata, "Phase Relation in SiC-Al4C3-B4C System at 1800°C," *J. Ceram. Soc. Japan*, **88** [6] 353-55 (1980).

[29] W.J. Moberlychan and L.C. De Jonghe, "Controlling Interface Chemistry and Structure to Process and Toughen Silicon Carbide," Acta Mater. **46** [7] 2471-77 (1998).

CHAPTER 4: Conclusions

Systematic study was carried out to investigate the effect of the aluminum additive amount on the microstructure development and room temperature mechanical properties of hot-pressed silicon carbide. Two complementary approaches, i.e. varying the aluminum content continuously or by steps, were employed.

An aluminum metal powder compact was enclosed in B- and C-doped SiC green compact and a continuous aluminum concentration gradient was successfully generated in the SiC after hot-pressing. As the distance to the original aluminum layer increases, the silicon carbide grains change from (a) elongated with bimodal grain size distribution to (b) uniformly elongated and then to (c) uniformly equiaxed. Both the bimodal region and the elongated region have higher toughness. The crack profiles show extensive crack deflection and crack wake bridging. On the other hand, regions with more equiaxed grains have lower fracture toughness. The cracks are transgranular and straight.

In light of the results of the continuous method, ABC-SiC with 3wt% to 7 wt% aluminum addition were hot-pressed to study the effect of the aluminum content on the microstructure and room temperature mechanical properties. A small variation of the aluminum content can drastically change the microstructure and hence the mechanical properties of silicon carbide. Grain boundaries of as hot-pressed SiC change from amorphous to crystalline as the aluminum content increases, which is presumably due to the change of the local chemical composition. The change of the nature of the grain boundaries results in a retarded β-to-α transformation. As a consequence, when the aluminum content varies from 3wt% to 7wt%, the elongated plate-like grains change as

follows: the aspect ratio increases about 6 times, the volume fraction decreases, the length increases first and then decreases with the peak at 5wt% aluminum addition. ABC-SiC with less than 5wt% aluminum addition has a high fracture toughness. The fracture toughness increases with the grain aspect ratio but decreases as the volume fraction of plate-like grains decreases. The fracture mode of plate-shaped grains depends on their orientation to the crack path. Fracture strength decreases with the increasing of grain size. ABC-SiC with 4 wt% aluminum addition shows the highest fracture toughness (6.3MPa$\sqrt{m}$) as well as high fracture strength (561MPa).

Ernest Orlando Lawrence Berkeley National Laboratory
One Cyclotron Road | Berkeley, California 94720

Prepared for the U.S. Department of Energy under Contract No. DE-AC03-76SF00098